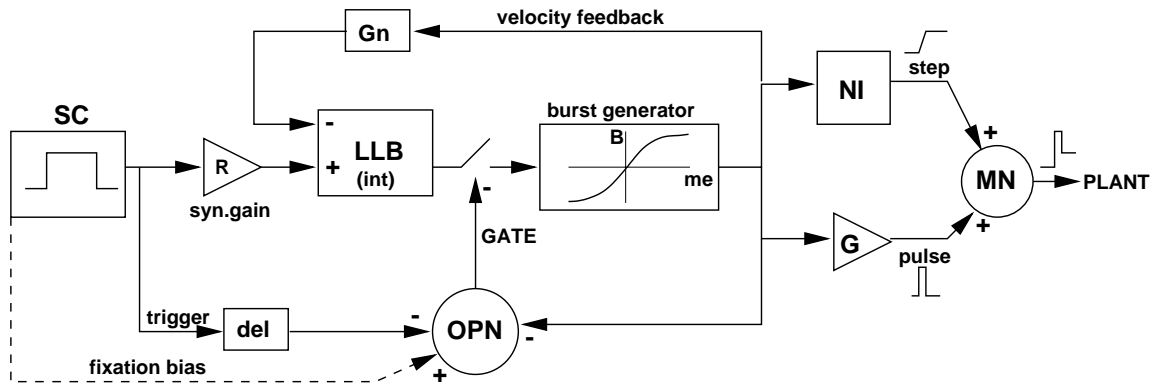


APPLYING SYSTEMS THEORY TO MODEL GAZE CONTROL



CoSMo Summerschool Groesbeek: June 29 - July 11, 2015

John van Opstal

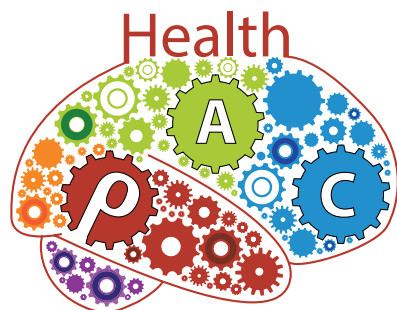
Dept. Biophysics, Donders Institute, Radboud Univ. Nijmegen, Netherlands

E-mail: j.vanopstal@donders.ru.nl

Web: <http://www.mbfys.ru.nl/~johnvo>

Donders Institute 
for Brain, Cognition and Behaviour

Radboud University Nijmegen



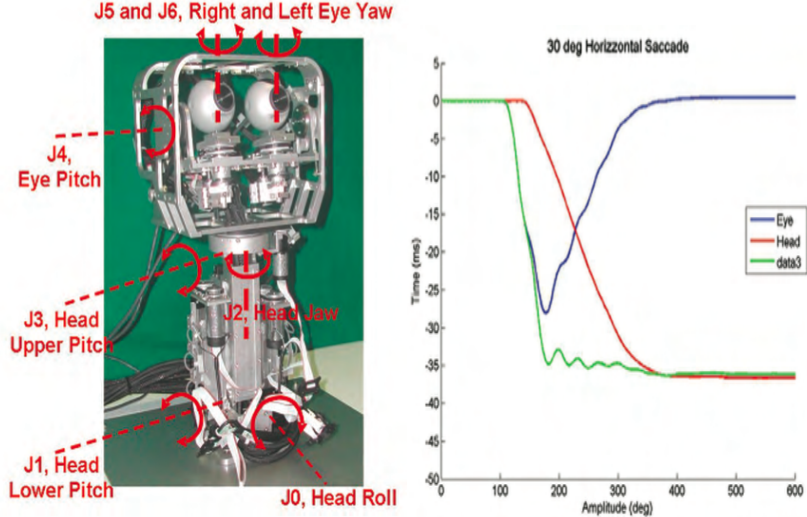

CAPNET
Canadian Action and Perception Network

Contents

1 June 30 (am): Intro Linear Systems Theory	3
1.1 Background (1.1-1.5 should preferably be studied in advance!)	3
1.2 Linearity	4
1.2.1 Impulse response and Step response	5
1.3 Transfer Characteristics: Fourier Analysis	7
1.3.1 Examples: Filters	10
1.3.2 Combining Linear Systems: Series, Parallel, Feedback	12
1.3.3 Example: Smooth pursuit eye movements	14
1.4 Transfer function: the Laplace Transform	15
1.4.1 A few Laplace examples	16
1.4.2 Poles and zeros	17
1.4.3 Systems with more poles and zeros	19
1.4.4 Poles and zeros for the slow-phase VOR	19
1.4.5 Pole-zero analysis of a feedback system	20
2 June 30 (pm): The Saccadic System	22
2.1 General background	22
2.2 Saccades	23
2.3 Neural Processes Underlying Saccade Generation	25
2.4 The Saccadic Brainstem Circuitry	26
2.5 Scudder's Model of the Saccadic System	31
3 June 30 (pm): The Computer Models	35
3.1 Part 1: PulseStep.mdl	35
3.2 Part 2: Saccade.mdl	38
4 Scudder revisited: common source and superior colliculus	41
4.1 Two-dimensional eye-movements: the Common Source Model	41
4.2 Neural mapping principles of the visual input	42
4.3 Sensorimotor mapping in the Superior Colliculus	43
4.3.1 The SC movement field	44
4.3.2 Population coding of saccades in the SC motor map	46
4.4 Exercises	48
5 The SC acts as a Vectorial Pulse Generator	49
5.1 The blink-perturbation paradigm in the SC	49
5.2 Spike-train analysis of SC saccade bursts: dynamic movement fields	51
5.3 The nonlinear vectorial pulse generator concept	57
5.4 Part 3: Computer simulations with saccade-lin.mdl: a nonlinear SC pulse generator	57

6 Extra Material: Intro Eye-Head Coordination	59
6.1 A problem for gaze control	59
6.2 Reference frames	60
6.2.1 Eye: driven by eye coordinates or head coordinates?	61
6.2.2 Coordinate transformations in eye-head gaze shifts	62
6.2.3 Eye-head gaze shifts: behavioral data	63
6.3 Gaze-control models	65
6.3.1 The PPRF output: eye- or gaze velocity?	66
6.4 The Eye-Head Computer Model	67
6.5 Gaze-control model 1: Goossens-Van Opstal (GVO97)	67
6.6 Appendix: Parameter listings of Simulink Gaze Models	69
6.7 Looking inside OMR, BG and VOR	71
6.8 Scudder's model revisited: GVO2011	74

7 Selected references	75
------------------------------	-----------



Robotic implementation (by Manfredi et al.) of one of the dynamic gaze-feedback control models discussed in this course. For further information, see: http://www.intechopen.com/source/pdfs/6241/InTech-Neurophysiological_models_of_gaze_control_in_humanoid-robotics.pdf

1 June 30 (am): Intro Linear Systems Theory

1.1 Background (1.1-1.5 should preferably be studied in advance!)

Biological systems are complex, yet highly organized. Trying to understand such systems in a quantitative sense, just a mere summing up of the different elements that comprise the system is inadequate, as the essential aspects of biological function reside in the *interactions* between many different subsystems.

Not surprisingly, a general theory for analyzing complex systems arose from the biological sciences. However, *Systems Theory* is by no means confined to biological systems. It has been applied successfully to a wide variety of disciplines: technical applications, physics, but also in the economic and social sciences.

A key element in Systems Theory is the use of so-called *Black-Box (BB) models*. A Black Box is an abstraction of the real problem of interest. The black box can only interact with the system's environment: the system communicates with the outside world by receiving signals (*inputs*), and it reacts to these inputs by creating its own signals which are in turn sent to the environment (*outputs*). The underlying structure of the system is *not* the object of study in pure systems analysis, but is (of course) eventually essential to fully understand the function of the (biological) system.

The main idea behind systems theory is that when the input-output relations of the Black Box are *identical* to those of the real system, than the BB model is *equivalent* to that system. In that case, quantitative predictions can be made on the basis of the BB model, to understand the system's behavior.



Fig. 1: A Black Box.

Systems Identification is the technique that aims to find the functional relationship between the input and output of the system. In abstract form:

$$y(t) = \mathcal{F}[x(t, \tau)]$$

which states that the output function (time-dependent) is some function of the input function (also time-dependent). \mathcal{F} is called a 'functional'.

In this short course we briefly review and discuss the methods used in Systems Theory. Although this involves some mathematics, understanding the technicalities is not essential to follow the main arguments. Students with a (slightly) deeper mathematical background, however, may want to try some of the more technical exercises that are mentioned in the text ('math'). All are encouraged to dive into the conceptual exercises ('all'). Answers provided against beer!

More importantly, all students should grasp the major *concepts*. In Linear Systems theory these are the system's *impulse response* and the *superposition principle*. From these two simple ideas we will derive some quite profound consequences:

1. From the impulse response one can predict the response of the LS to *arbitrary* signals (through *convolution*).
2. From the Superposition Principle it follows that the sinusoid (harmonic signal) is the *only* signal that is preserved by the system (harmonic signals are *Eigenfunctions* of LS).
3. The latter property leads to Fourier Analysis and the system's *Transfer Characteristic*.
4. Any combination of Linear Systems forms by itself again a LS.
5. Through the *Laplace Transform*, both the impulse response **and** the transfer characteristic can be readily obtained (from a *zero-pole analysis*, without much math....)

We then apply these ideas to some real-world examples: (i) a quantitative model of the oculomotor plant, (ii) the slow-phase vestibular ocular reflex, (iii) more in depth: the saccadic eye-movement system.

In the afternoon we apply this knowledge to the more complex problem of generating saccadic eye movements. All models are implemented as Simulink applications in Matlab; there will be afternoon practicum sessions, in which we develop a feeling for the way in which Systems Theory helps us to study complex (neuro-)biological systems.

Overview:

We first discuss the concepts of *Linearity*, and *Linear Systems Theory*. The following concepts will be introduced and further derived: *the Impulse and Step Response*, *Convolution*, *Harmonic Eigenfunctions*, *Fourier Analysis*, the *Transfer Characteristic*, and *Feedback control*. We end with a brief introduction of the *Laplace Transform*, and it's associated *Pole-Zero analysis*. **Those who are proficient in these concepts will briefly want to glance over this stuff; the others are strongly encouraged to prepare in advance, and try to get at least the problems clear!**

1.2 Linearity

A system is linear, when its response to a weighted sum of an arbitrary number of inputs, is exactly equal to the *same* weighted sum of the system's responses to each of the individual inputs.

In math: if the system's responses to a set of input signals, $x_k(t)$ is given by $y_k(t)$, and suppose we create a new input signal as follows: $x(t) = \sum_k a_k \cdot x_k(t)$, with a_k arbitrary constants ('weights'), then linearity requires that the system's response equals: $y(t) = \sum_k a_k \cdot y_k(t)$.

Note that the output's weighting constants should be identical to the input weightings! This strict requirement, called the *Superposition Principle*, is quite nontrivial, as it is often violated in real systems (as we will see).

Exercise 1 (all): Suppose a system that transforms input $x(t)$ according to:

$$y(t) = a \cdot x(t) + b$$

with a and b arbitrary, real constants.

In other words, the relation between the system's output $y(t)$ and its input $x(t)$ is described by a straight line. Is the system linear? An important related question: do two such systems with different parameters, say $y_1 = ax + b$ and $y_2 = cx + d$ with a, b, c, d unequal and nonzero commute? (i.e., $y_1(t) \cdot y_2(t) = y_2(t) \cdot y_1(t)?)$

Exercise 2 (all): Suppose that the input-output relation of a system is given by:

$$y(t) = a \cdot x^2(t) + b$$

Show that this system can never be linear if $a \neq 0$.

1.2.1 Impulse response and Step response

An important consequence of the Superposition Principle is the following:

All linear systems are *fully characterized by their Impulse Response.*

Definition: The impulse response of a (linear) system is the time evolution of the system's response when its input is a so-called Dirac impulse function:

$$x_D(t) \equiv \delta(t) = \begin{cases} \infty & \text{for } t = 0 \\ 0 & \text{for } t \neq 0 \end{cases} \Rightarrow \int_{-\infty}^{\infty} f(t) \cdot \delta(t - \tau) \cdot dt = f(\tau) \quad (1)$$

That is, the Dirac impulse is infinitely high at $t = 0$, and zero for all other times. Its area is defined to be exactly one. Especially the right-hand integral property is crucial for what follows below. Note that the impulse is a mathematical idealization of a narrow *pulse* ('spike') with width ΔT and height $1/\Delta T$. In the limit of $\Delta T \rightarrow 0$ we have Dirac's proposal.

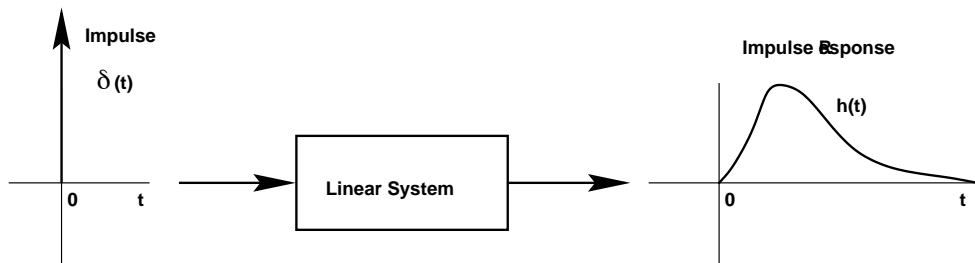


Fig. 2: The impulse response of an arbitrary linear system can be quite a rich signal!

The reason for its importance in Linear Systems Theory is the integral property of Eq. 1. As illustrated Fig. 3, an arbitrary signal $x(t)$ can be constructed by a sequence of discrete pulses, each with their own height (this is the Riemann sum, used to derive integration in calculus!). The height of the pulses is given by the mean signal value within the pulse.

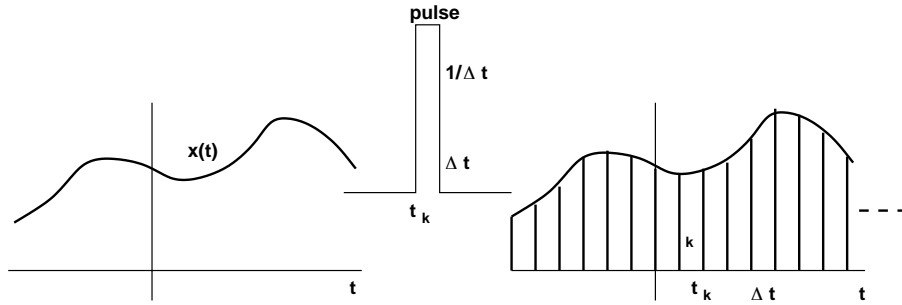


Fig. 3 Any signal can be described by a series of pulses (the Riemann sum).

Mathematically, the integral property of the Dirac function (Eqn. 1) can be reformulated as follows: suppose an arbitrary input signal, $x(t)$, we write it as:

$$x(t) = \int_{-\infty}^{\infty} x(\tau) \cdot \delta(t - \tau) \cdot d\tau \quad (2)$$

where we merely changed the 'dummy' integration variable t of Eqn. 1 into τ . Although a seemingly trivial exchange, Eqn. 2 can be interpreted as: any signal $x(t)$ can be described by a superposition of Dirac pulses at different times, each weighted with the signal's value at those times!

As a consequence, and according to the superposition principle, (and here it comes!), *the response of the linear system to such a weighted sum of impulses, will be the same weighted sum of individual impulse responses!* In other words, if we know the response of the system to a single impulse, let's call it $h(t)$, we can exactly predict its response to an *arbitrary* input! We now write this important statement as follows:

$$y(t) = \int_{-\infty}^{\infty} x(\tau) \cdot h(t - \tau) \cdot d\tau \quad (3)$$

This result is called the *convolution integral*. Thus, we *fully understand* the system's behavior in a scientifically sound sense!

We will now make only a small adjustment to this important equation: from now on we only consider so-called *causal* systems. Such systems only respond *after* an input has been applied (there is only an effect to a cause!). Mathematically, this means that the impulse response function, $h(t)$, is zero for all $t < 0$.

Exercise 3 (math): Now show that by a simple change of variables, the convolution integral can be rewritten in the following form:

$$y(t) = \int_0^{\infty} x(t - \tau) \cdot h(\tau) \cdot d\tau \quad (4)$$

This is the form in which the convolution integral is usually represented.

Exercise 4 (all): Give a conceptual interpretation of all the elements in this equation (i.e., the meaning of: t , τ , $\tau = 0$, $\tau = \infty$, $x(t - \tau)$, and $h(\tau)$)

Exercise 5 (all): Now that we know that linear systems are typically not just straight-line relationships between input and output, write the linear system $y(t) = a \cdot x(t)$ as a convolution integral (what is its impulse response?).

Example:

An important application of the above is the following. Suppose that the input signal a *unity step*, $U(t)$: this signal is zero for all $t < 0$ and one for $t \geq 0$. The response of the linear system to a step is the *step response*.

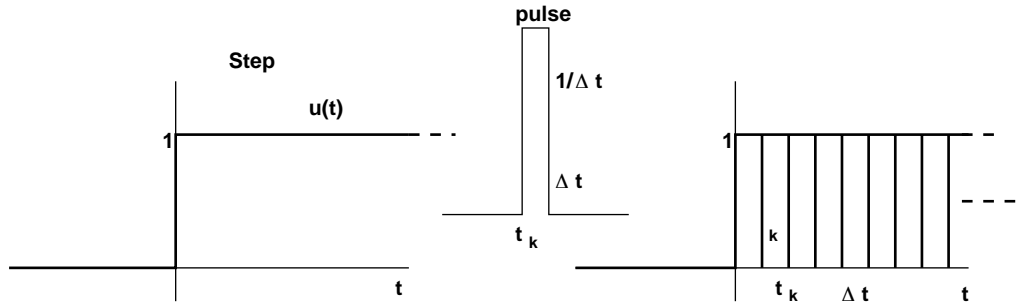


Fig. 4: The step function can be considered as the sum of a sequence of pulses with weighting factor 1.

Consider now that the unit step function can also be regarded as the cumulative integral of the impulse function:

$$U(t) = \int_{-\infty}^t \delta(\tau) d\tau \quad (5)$$

Indeed, for $t < 0$ the step is still zero. At $t = 0$ it is suddenly 1 (i.e., the impulse's area) and then stays at this value forever. From this it follows that the system's *Step response* is the *cumulative integral* of the system's impulse response:

$$s(t) = \int_0^t h(\tau) d\tau \quad (6)$$

Exercise 6 (math): Show that Eqn. 6 indeed follows from Eqn. 4.

Note, that the reverse is also true: it is straightforward to determine the Impulse response from the system's Step response, by taking its *derivative* with respect to time:

$$h(t) = \frac{ds}{dt} \quad (7)$$

1.3 Transfer Characteristics: Fourier Analysis

The description of linear systems and signals has so far been given in the *time domain*. However, in practice it is often not the most convenient way to study linear systems, as the mathematics involved (time integration) can be quite tedious and time consuming.

However, there is an interesting and elegant alternative, which is also a consequence of superposition. In the previous section we have seen that any signal can be arbitrarily well approximated by a sequence of impulses. Here, we will discuss that signals can also be approximated by other elementary functions, in particular, by *sinusoids of different frequencies*. In such a description, one resorts the analysis to the *frequency domain*. Here, we will dwell on this possibility a little further, as it is a commonly used technique for analyzing linear systems. An important reason for this is that the mathematics involved turns out to be surprisingly simple (algebraic multiplication and division, instead of integration).

It is important to realize that the descriptions of signals and systems in the time domain and in the frequency domain are just two sides of the same coin. That is, they are fully equivalent, and linked through elementary mathematical transformations that can be expressed in each other's domain. The technique that does the translation from time domain to frequency domain and vice versa is called *Fourier analysis*.

We are first going to show that sines and cosines are indeed very special functions for linear systems. In fact, they are the *only* signals that do not change their shape when passed through a linear system! (note: we saw before that the Dirac impulse is completely distorted by the system, as the general impulse response function doesn't look like an impulse at all!). In other words: sines and cosines are so-called *Eigenfunctions* of linear systems. Here's the lemma:

For $x(t) = \sin(\omega \cdot t)$, with $\omega \equiv 2\pi f$ the angular frequency, and $f = 1/T$ the sine's frequency (T its period), the output of any linear system is:

$$y(t) = G(\omega) \cdot \sin(\omega \cdot t + \Phi(\omega)) \quad (8)$$

Here, $G(\omega)$ is the system's amplitude characteristic (or *gain*), and $\Phi(\omega)$ is its phase characteristic, both of which depend on the sine's frequency (see below). In other words, a crucial test for linearity is to demonstrate that '*sine in*' gives '*sine out*', or: the output of the linear system to a sine can only yield a sine with the *same* frequency. Only the amplitude and phase of the output sine may differ from the input!

Excercise 7 (all): Verify that the systems given by $y(t) = a \cdot x(t) + b$ and $y(t) = a \cdot x^2(t) + b$ indeed violate this important test!

Excercise 8 (math): Now use the convolution integral, and $\sin(x \pm y) = \sin(x) \cos(y) \pm \cos(x) \sin(y)$ to prove Eqn. 8, and that

$$G(\omega) = \sqrt{A(\omega)^2 + B(\omega)^2} \quad \text{and} \quad \Phi(\omega) = -\arctan B(\omega)/A(\omega)$$

where

$$A(\omega) = \int_0^\infty h(\tau) \sin(\omega\tau) d\tau \quad \text{and} \quad B(\omega) = \int_0^\infty h(\tau) \cos(\omega\tau) d\tau \quad (9)$$

In other words, the amplitude and phase characteristics are both a function of frequency, and they are fully determined by the system's impulse response!

Eqn. 9 represents the so-called *Fourier transform* $H(\omega)$, of the system's impulse response, $h(t)$. It states that the impulse response (any integrable function, for that matter) can be represented by a sum of weighted sines and cosines, where the function itself acts as the weighting. Note that the Fourier transform consists of *two* functions, determined by sine and cosine respectively, that together represent a *vector* in two-dimensional space: $(x, y) = (R \cos(\phi), R \sin(\phi))$. Without becoming too technical here, such a vector can be conveniently represented by a *complex number*: $z \equiv x + iy = R \cdot (\cos(\phi) + i \cdot \sin(\phi)) \equiv R \cdot \exp(i\phi)$. Without proof, we here pose that the Fourier Transform $X(\omega)$

of a (integrable) signal, $x(t)$, is defined by:

$$X(\omega) = \int_{-\infty}^{\infty} x(t)e^{-i\omega t} dt \quad (10)$$

with i the complex unit (the imaginary number), defined by $i^2 \equiv -1$.

The Fourier transform is a complex function, consisting of a real part (the cosine) and an imaginary (the sine) part:

$$X(\omega) = \text{Real}(X(\omega)) + i \cdot \text{Imaginary}(X(\omega))$$

. This is most conveniently written as:

$$X(\omega) = R(\omega) \cdot e^{i \cdot \phi(\omega)} \quad (11)$$

where we call $R(\omega)$ the magnitude and $\phi(\omega)$ the phase of the signal. This ingenious identity follows from Euler's equation that relates exponential functions to sines and cosines through:

$$e^{i\phi} = \cos(\phi) + i \cdot \sin(\phi) \quad (12)$$

We're now only a small step away from showing that with Fourier Analysis it is possible to compute the output of the linear system through a simple algebraic multiplication of the Fourier Transforms of signal $x(t)$ and the system's impulse response $h(t)$:

$$Y(\omega) = H(\omega) \cdot X(\omega) \quad (13)$$

Exercise 9 (math): Prove this very important equation by applying the Fourier Transform to Eqn. 4. (Hints: use the causality principle: $h(t) = 0$ for $t < 0$. Also: keep track of the dummy integration variables!).

A consequence of this simple rule is that combinations of linear systems can be easily analyzed. In what follows below, we will describe how this works. First, let's apply the exponential representation of the Fourier transforms to Eqn. 13:

$$Y(\omega) \equiv R_Y(\omega) \cdot e^{i\phi_Y(\omega)} = G(\omega) \cdot e^{i\Phi(\omega)} \cdot R_X(\omega) \cdot e^{i\phi_X(\omega)} = G(\omega) \cdot R_X(\omega) \cdot e^{i \cdot (\Phi(\omega) + \phi_X(\omega))}$$

The analysis takes place in the *frequency domain*, and relies on the system's *transfer characteristic* $H(\omega)$. Like the impulse response in the time domain, the transfer characteristic in the frequency domain provides a *complete* characterization of the linear system!

Definitions: The *gain* (= magnification) of the system is defined by the quotient between the output and input amplitudes for each frequency, and the phase shift by the phase difference between output and input phases, respectively:

$$G(\omega) \equiv R_Y(\omega)/R_X(\omega) \quad \text{and} \quad \Phi(\omega) = \phi_Y(\omega) - \phi_X(\omega) \quad (14)$$

The transfer characteristic, $H(\omega) = [G(\omega), \Phi(\omega)]$ tells at a glance what properties the linear system has. It is often more insightful as the corresponding impulse response in the time domain. Of course, there is a unique relationship between these two representations, as they both fully characterize the system.

1.3.1 Examples: Filters

Some important transfer characteristics that are frequently encountered in models of biological systems are:

- The Low-Pass (LP) characteristic: such a system lets sines/cosines with *low* frequencies pass well (i.e. at high gain, and small phase shift), but almost entirely stops high frequencies. As an example, the simplest model of the oculomotor plant is a first-order low-pass filter (time constant $T_E \approx 150$ ms), for which the impulse response function and the associated transfer characteristic are:

$$h_E(t) = \frac{1}{T_E} \cdot e^{-t/T_E} \quad \text{and} \quad H_E(\omega) = \frac{1}{1 + i\omega T_E}$$

Exercise 10 (math): Verify the right-hand Fourier Transform, and that its Gain and Phase characteristics are given by:

$$G_E(\omega) = \frac{1}{\sqrt{1 + \omega^2 T_E^2}} \quad \text{and} \quad \Phi_E(\omega) = -\arctan(\omega T_E)$$

Plot these characteristics and verify that this indeed describes a Low-Pass system. When the Gain Characteristic is plotted on log-log scale, and the Phase characteristic on log-linear scale, the resulting graph is called a *Bode Plot*. The advantage of taking the logarithm of the amplitude is that multiplication and division then simply change to graphical addition/subtraction.

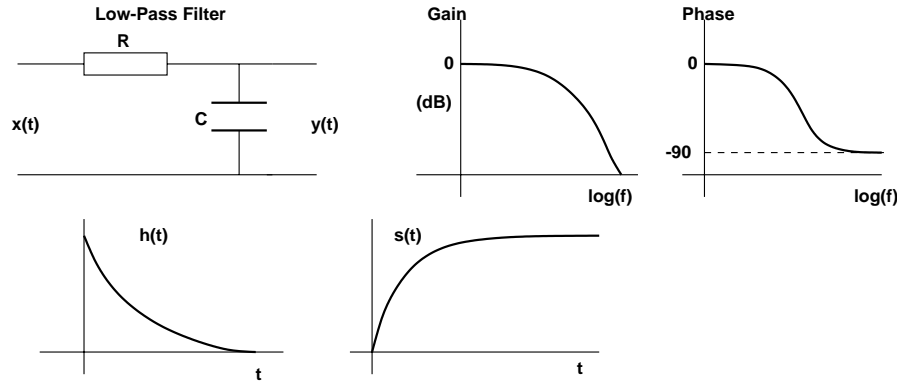


Fig. 5: Example of a simple LP system: a resistor, R , in series with a capacitor, C . The output is measured across the capacitor. High frequencies are strongly attenuated, and are lagged in phase by 90 deg, while low frequencies pass without change. Also the impulse and step responses of the system are shown.

- The High-Pass (HP) characteristic does the reverse: *high* frequencies pass well, while the low frequencies are stopped. Note that the impulse response of such a system is thus given by:

$$h_{HP}(t) = \delta(t) - h_{LP}(t) = \delta(t) - \frac{1}{T_V} \cdot e^{-t/T_V} \quad \Rightarrow \quad H_{HP}(\omega) = 1 - H_{LP}(\omega) = \frac{i\omega T_V}{1 + i\omega T_V}$$

Exercise 11 (math): Show that its Gain and Phase characteristics are given by:

$$G(\omega) = \frac{\omega T_V}{\sqrt{1 + \omega^2 T_V^2}} \quad \text{and} \quad \Phi(\omega) = \arctan(1/\omega T_V)$$

The slow-phase response of the Vestibular system can be approximated by such a filter. The time constant of the VOR is about $T_V \approx 20$ s. Plot these characteristics and verify that this describes a High-Pass system.

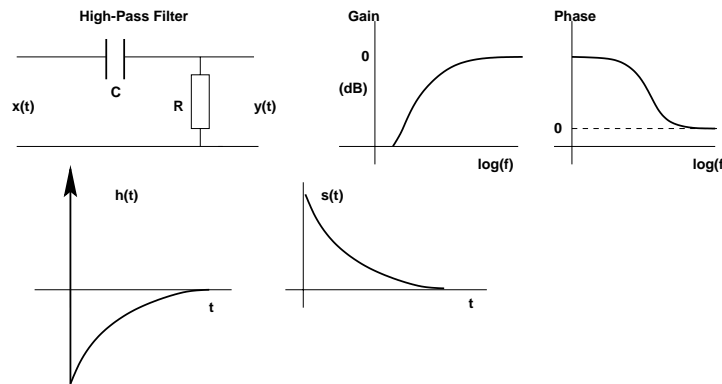


Fig. 6: Example of a simple HP system: now the voltage across the resistor is the circuit's output.

- The Band-Pass (BP) characteristic: only sines/cosines with frequencies within a limited range (the pass band) are passed; all other frequencies are stopped.
- The Band-Stop (BS) characteristic does the reverse of the BP system: frequencies within the stop band are stopped, all others are passed.
- The Time Delay: all frequencies are passed equally well ('All Pass'), but each sine/cosine is passed with a fixed time delay: ΔT : $y(t) = x(t - \Delta T)$.
- The Integrator: time-integrates the input. It functions as a LP system (see below).
- The Differentiator: time-differentiates the input. Acts like a HP system (see below).

Without having to use advanced mathematics and Fourier analysis it is sometimes straightforward to compute the transfer characteristic of some simple (and useful) linear systems. Try the following assignments:

Exercise 12 (all): Consider a pure integrator system:

$$y(t) = \int_0^t x(\tau) \cdot d\tau$$

- Show that this is indeed a *linear* system.
- What is the impulse response?

- (c) What is the step response?
 (d) Now take $x(t) = A\sin(2\pi ft)$ as the input for this system. Compute the amplitude and phase of the output, $y(t)$. (N.B. these are functions of f !) This immediately gives us the transfer characteristic of the system!
 (e) Why is this a LP system. Why is the LP system of the figure (above) a so-called 'leaky integrator'?

Exercise 13 (all): Consider the differentiator:

$$y(t) = \frac{dx(t)}{dt}$$

- (a) Show that this is a *linear* system.
 (b) What is the impulse response?
 (c) What is the step response?
 (d) Compute (like in problem 4) the transfer characteristic of this system.
 (e) Why is the HP system of the figure above a leaky differentiator?

Exercise 14 (all): Consider the pure time delay:

$$y(t) = x(t - T)$$

Answer the same questions (a - d) as in the previous problems.

1.3.2 Combining Linear Systems: Series, Parallel, Feedback

Any combination of linear systems results in a new linear system.

Here, we will focus on three combinations, which will all figure in our model of the saccadic system:

- the series concatenation
- the parallel combination
- "feedback". Especially this is an important circuit in biological systems.

Series concatenation

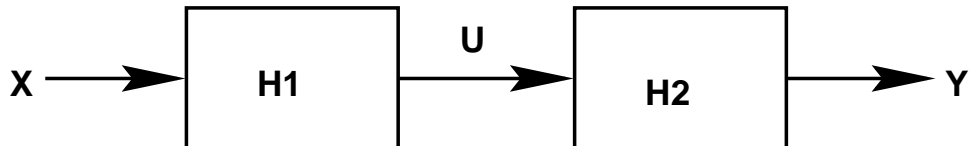


Fig. 7: Two linear systems connected in series.

To determine the overall transfer of the system, the general approach is to introduce a dummy signal. Here, we add signal U as the output of system H_1 , which is now also the input for system H_2 . It can now be readily verified that by using the multiplication rule, the output Y , and input X are related through:

$$Y = H_1 \cdot H_2 \cdot X \Rightarrow H(\omega) = H_1(\omega) \cdot H_2(\omega) \quad 15$$

Exercise 15 (all): Consider a LP and HP system, with characteristics as shown above. What can you tell about the total transfer characteristic if the systems are connected in series? Distinguish different cases!

Parallel connection

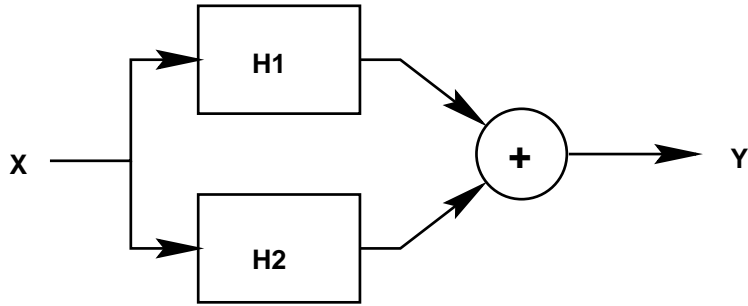


Fig. 8: Two linear systems, connected in parallel.

It is quite straightforward to show that in this case the total transfer characteristic will be given by:

$$Y = (H_1 + H_2) \cdot X \quad (16)$$

Exercise 16 (all): Discuss the total characteristic if the LP and HP systems are connected in parallel.

Feedback

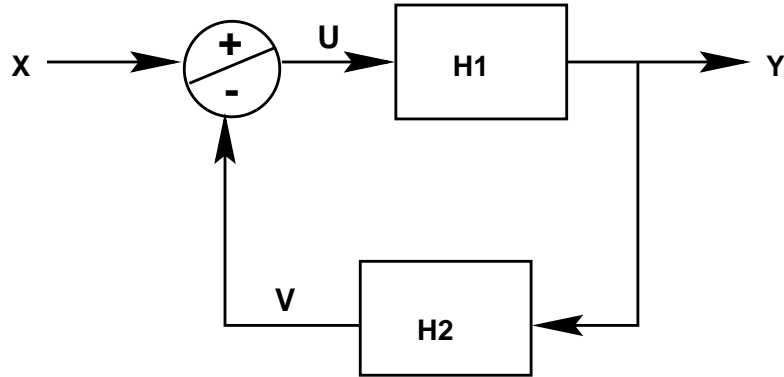


Fig. 9: Two linear systems forming a feedback system.

To determine the total transfer characteristic of the feedback system, we introduce two dummy signals: U results from the addition/subtraction operation, and V is the output of system H_2 .

$$\begin{aligned}
 \text{it then follows that } & Y = H_1 \cdot U \\
 \text{while } & U = X - V \\
 \text{and } & V = H_2 \cdot Y
 \end{aligned}$$

The total transfer of the system, $\frac{Y}{X}$, is then (but verify!):

$$\frac{Y(\omega)}{X(\omega)} \equiv H(\omega) = \frac{H_1(\omega)}{1 + H_1(\omega) \cdot H_2(\omega)} \quad (17)$$

Feedback forms an essential feature of complex, biological systems. There must be a good reason for using feedback! In fact, there are many. Here, we name just a few:

A first important advantage can be appreciated if we were to assume that for the relevant part of the spectrum the following would be true: $H_1(\omega) \cdot H_2(\omega) \gg 1$. In that case Eqn. 17 will simply reduce to:

$$H(\omega) = \frac{1}{H_2(\omega)} \quad (18)$$

In other words:

The system's transfer is *independent of the system in the feedforward path!*

This is a very powerful property! Suppose, that we have a subsystem with highly variable properties (e.g. vulnerable components, large variations in gain, prone to fatigue, etc.). Then feedback ensures that the transfer of the total system will still be highly reliable.

From Eq. 18 we note a second important advantage of feedback:

In a feedback system with a high feedforward gain $H_1(\omega)$ the system's transfer is the *inverse* of the feedback transfer $H_2(\omega)$. Thus:

H_2	then	H
Integrator	\Leftrightarrow	Differentiator
Differentiator	\Leftrightarrow	Integrator
Low-pass filter	\Leftrightarrow	High pass filter
High-pass filter	\Leftrightarrow	Low pass filter

1.3.3 Example: Smooth pursuit eye movements

The *smooth pursuit eye movement system* serves to precisely follow moving visual targets, and to keep them stabilized on the fovea. Input to the system is the *velocity* of the target across the retina,; it is also called the *retinal slip velocity*. The output of the system is the eye velocity. The system aims to minimize retinal slip, i.e. to equal target velocity and eye velocity.

Note that we have a system with negative feedback, in which the feedback is 'automatically' provided by the eyes' own motion (see figure).

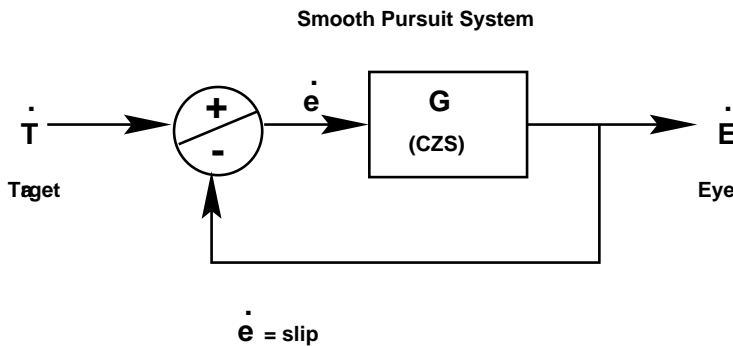


Fig. 10: A simple model of the ocular smooth pursuit system.

The transfer characteristic of this system is given by:

$$\frac{\dot{E}}{\dot{T}} \equiv G_{tot.} = \frac{G}{1+G}$$

With G the feedforward gain of the system. It is also called the *open-loop gain* of the system: that magnification of the input signal, if the feedback would be eliminated. The open-loop gain may be supposed to be somehow embodied by systems within the brain. It would therefore be interesting to be able to perform experiments to measure the properties of G .

The system tries to equal \dot{E} and \dot{T} , i.e. $\dot{e} = 0$. For that to work, the total transfer, G_{tot} should be close to 1, and the system's feedforward gain, G , should have to be large (why?). The following experiment allows one to measure G directly:

1. The eye which sees the stimulus movement is temporarily paralyzed.
2. The eye movement of the non-paralyzed, but *covered* eye is measured.

Exercise 17 (all): Argue why we can indeed measure the open-loop gain G with this experiment (it turns out to be approximately 20).

1.4 Transfer function: the Laplace Transform

The Fourier Transform (Eq. 10) requires that the integral can be performed, in other words, the signal should be integrable. For transient signals this is always the case, but one very important problem with the Fourier transform is that one of the most common signals, the unity step function, $U(t)$, has no Fourier transform! This is why:

$$U(\omega) = \int_{-\infty}^{\infty} U(t) e^{-i\omega t} dt = \int_0^{\infty} e^{-i\omega t} dt = -\frac{1}{i\omega} e^{-i\omega t} \Big|_0^{\infty}$$

which is not defined. This problem is solved by using different basis functions to approximate the signal. Instead of sines and cosines, the Laplace Transform uses exponentially decaying sines and cosines, i.e. both real and imaginary exponentials, by setting:

$$e^{st} \quad \text{with } s \equiv \sigma + i\omega \quad \text{the complex frequency}$$

with real part σ and imaginary part ω . To visualize what this means, let's introduce the complex s -plane:

Every point on the plane represents a waveform $\exp(st)$ as shown. In the right-half plane $\sigma > 0$ and $\exp(\sigma t)$ blows up. Equivalent to the Fourier transform, which is an infinite sum of weighted imaginary exponentials, the Laplace Transform, $F(s)$, is defined as an infinite sum of weighted complex exponentials:

$$\mathcal{L}[f(t)] \equiv F(s) = \int_0^\infty f(t)e^{-st}dt \quad (19)$$

So it appears that compared to the Fourier transform, we have just replaced $i\omega$ with s , and the time integration runs for positive values only, as $F(s)$ only uses $f(t)$ for $t > 0$; this is not a serious restraint.

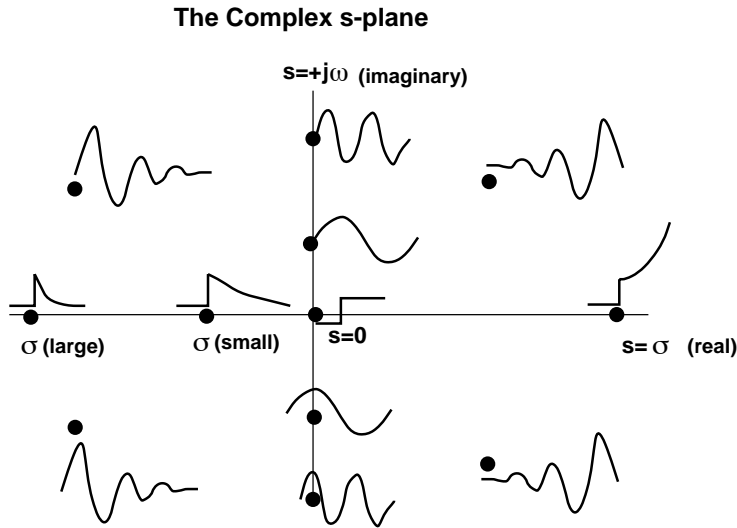


Fig. 11: The complex s -plane: complex exponentials.

1.4.1 A few Laplace examples

The unit step function, $f(t) \equiv U(t)$ can now be readily represented:

$$\mathcal{L}[U(t)] = \int_0^\infty U(t)e^{-st}dt = -\frac{1}{s}e^{-st}\bigg|_0^\infty = \frac{1}{s} \quad (20)$$

As usual, if we have the transform for one waveform, we have it for all related waveforms such as its derivative and its integral. For the derivative, differentiate under the integral with respect to t :

$$\mathcal{L}\left[\frac{df}{dt}\right] = s \cdot F(s) - f(0+) \quad (21)$$

where $f(0+)$ is the function's initial condition. In short, to differentiate, multiply by s , and to integrate, multiply by $1/s$ (indeed, $1/s$ is the representation of the unit step, which is the integral of the Dirac impulse!)

So the transform of the Dirac delta pulse (the derivative of the step) is $F(s) = 1$, and the transform of the ramp (the integral of the step) is $F(s) = 1/s^2$.

From now on we will put transfer functions into Laplace notation, $H(s)$, rather than in Fourier notation, $H(\omega)$. Like for Fourier transforms, it can be readily verified that the output of a linear system in Laplace notation is also found by algebraic multiplication:

$$Y(s) = H(s) \cdot X(s) \quad (22)$$

Another very common signal is $\exp(-at)$ (e.g. the impulse response of a Low-Pass system, see above). To find its Laplace transform:

$$\mathcal{L}[e^{-at}] = \int_0^\infty e^{-(a+s)t} dt = \frac{1}{s+a} \quad (23)$$

To use this new concept, let's look at the first-order oculomotor plant model once more. Its impulse response was given by:

$$h_E(t) = \frac{1}{T_E} e^{-t/T_E}$$

and now let's take its \mathcal{L} :

$$H_E(s) = \frac{1}{1+sT_E} \quad (24)$$

is the plant's transfer function in Laplace notation. We didn't seem to have gained anything new, but note that we can now readily determine the system's step response, by applying Eqn. 22:

$$Y_{step}(s) = H_E(s) \cdot \frac{1}{s} = \frac{1}{s \cdot (1+sT_E)} \quad (25)$$

To find the step response in the time domain, we only need to find the inverse transform. Here we won't go into the mathematical details of computing inverse Laplace transforms by integrating in the complex plane. Instead, we use a simple trick, by rewriting the Laplace function into familiar terms for which we simply know the time-evolution. In this case, we use basic algebra as follows:

$$\frac{1}{s \cdot (1+sT_E)} = \frac{A}{s} + \frac{B}{1+sT_E} \quad (26)$$

and determine A and B . The student should check that this yields: $A = 1$ and $B = -T_E$. So:

$$Y_{step}(s) = \frac{1}{s} - \frac{T_E}{1+sT_E} = \frac{1}{s} - \frac{1}{s+1/T_E} \quad (27)$$

where we put the right-hand term into the format of Eqn. 23! Inverse transformation is now trivial:

$$s(t) = U(t) - e^{-t/T_E} \quad (28)$$

Note that this holds for $t \geq 0$ and that this is indeed the system's step response. We now introduce a very useful graphic aid for system's analysis: the use of poles and zeros of the Laplace Transform.

1.4.2 Poles and zeros

Note that the LP transfer characteristic $H(s) = 1/(sT + 1)$ becomes infinite when $s \rightarrow -1/T$. Now mark this spot in the s -plane with an X. It's called a *pole*.

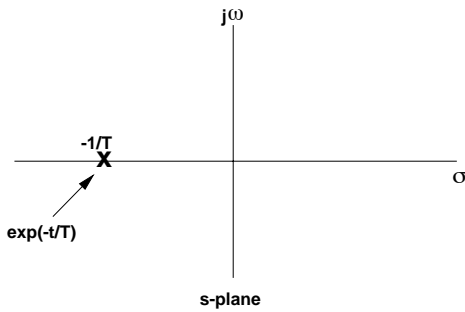


Fig. 12: The pole of a low-pass filter

Interestingly (and not by accident!), this point on the real axis of the *s*-plane also represents the *impulse response* signal $\exp(-t/T)$ of the system! So, in fact, the pole location tells you everything you need to know about this system, as it totally characterizes the system's dynamics. People have therefore decided to let the pole-zero diagram represent the system, rather than the mathematical expressions in time, frequency, or Laplace domains.

There is an immediate relationship between the pole-zero diagram and the original Fourier frequency (Bode) plot, when we realize that both are an analysis of the *frequency response* of the system. Fourier analysis measures the system's response to sines of different frequencies. In the Laplace *s*-plane these sines are located on the imaginary axis: $\exp(i\omega)$. To find the system's frequency response to arbitrary sines we choose a frequency, say ω , and determine its distance to the location of the poles (and zeros) in the *s*-plane. Here's how it works for the simple LP system:

The distance, ρ , between the pole and test frequency ω is

$$\rho = \sqrt{\omega^2 + (1/T)^2} \text{ and its reciprocal: } \frac{1}{\rho} = \frac{1}{\sqrt{1 + (\omega T)^2}} \quad (29)$$

gives us the *gain* of the system! Similarly, the angle of the line with the positive real σ axis is:

$$\tan(\theta) = \frac{\omega}{(1/T)} = \omega T \quad (30)$$

which gives the LP system's phase-lag (for poles, we add a minus sign to the angle)! As the test point moves up along the $j\omega$ axis (i.e. higher frequencies), the gain $1/\rho$ goes down and the phase angle approaches -90° , just as we found in the Bode diagram. Thus, the pole-zero diagram gives an immediate graphic portrayal of the system's frequency behavior too, without having to do any Fourier analysis!

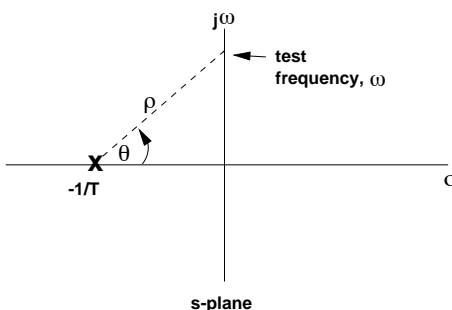


Fig. 13: Reconstruction of the LP Bode plot from the pole

1.4.3 Systems with more poles and zeros

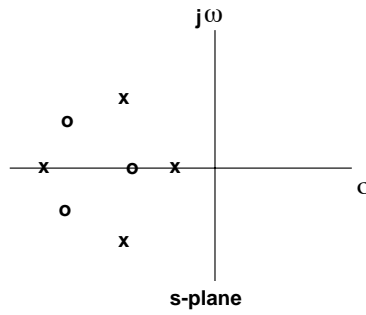
Without proof, we here pose that Laplace transfer characteristics of linear systems will have the following general appearance:

$$H(s) = \frac{a_n s^n + a_{n-1} s^{n-1} + a_{n-2} s^{n-2} + \cdots + a_1 s + a_0}{b_m s^m + b_{m-1} s^{m-1} + b_{m-2} s^{m-2} + \cdots + b_1 s + b_0} \quad (31)$$

which is a ratio of two polynomials in s . The numerator will have n zeros, call them $-z_1, -z_2, \dots, -z_n$. The denominator will have m poles, $-p_1, -p_2, \dots, -p_m$. So, it is possible to write:

$$H(s) = \frac{(s + z_1)(s + z_2) \cdots (s + z_n)}{(s + p_1)(s + p_2) \cdots (s + p_m)} \quad (32)$$

Graphically, this can be represented by the pole-zero diagram.

**Fig. 14:** Complex poles are always conjugate

Poles and zeros lying off the real axis are complex and will always occur in conjugate pairs. In this way, the imaginary parts will cancel out, leaving only the real (oscillatory) wave form in the time domain.

1.4.4 Poles and zeros for the slow-phase VOR

The impulse response of the slow-phase VOR is (see above):

$$h_V(t) = \delta(t) - \frac{1}{T_V} \cdot e^{-t/T_V} \quad (33)$$

We readily obtain its Laplace transform:

$$\mathcal{L}[h_V(t)] = 1 - \frac{1}{1 + sT_V} = \frac{sT_V}{1 + sT_V} \quad (34)$$

from which we find a *pole* at $s = -1/T_V$ and a *zero* at $s = 0$. To obtain the gain of the frequency-transfer characteristic we note that:

$$G_V(\omega) = \frac{\rho_N(\omega)}{\rho_P(\omega)} = \frac{\omega T_V}{\sqrt{1 + \omega^2 T_V^2}} \quad (35)$$

and for the phase characteristic:

$$\Phi_V(\omega) = \Phi_N(\omega) - \Phi_P(\omega) = \frac{\pi}{2} - \arctan \omega T_V \quad (36)$$

What is the step response of the slow-phase VOR? I.e., how does the VOR respond to a constant head velocity (\dot{h}_0) starting at $t = 0$? We multiply the Laplace transfer characteristic by $1/s$ and find:

$$H_{V(\text{step})}(s) = \frac{\dot{h}_0 T_V}{1 + s T_V} = \frac{\dot{h}_0}{s + 1/T_V} \quad (37)$$

It is immediately clear that the step response of slow-phase eye velocity in time is an exponential decay with a time constant of T_V : $\dot{e}_S(t) = \dot{h}_0 \cdot \exp(-t/T_V)$. Exactly what would be expected for a high-pass system.

In summary: the Laplace transform (the transfer characteristic and the pole-zero analysis) allows for a rapid, graphical and complete assessment of the system's properties, and to calculate its response to a variety of stimuli without tedious and technical calculations.

Question 18: Now consider the following interesting problem: The step response of the VOR decays exponentially with a time constant of $T_{\text{VOR}} \sim 20\text{s}$. Design an input such that the response of the VOR is a step (in other words, never decays, the eyes keep moving at a constant speed in the head!)

1.4.5 Pole-zero analysis of a feedback system

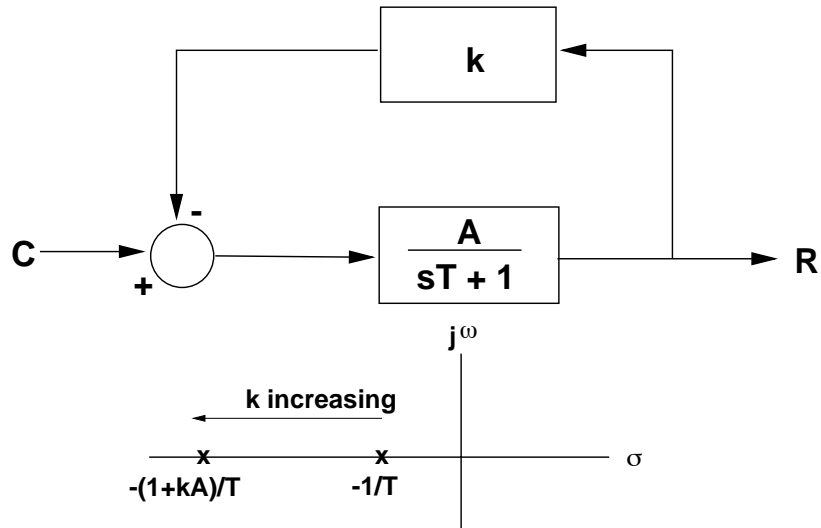


Fig. 15: Effect of varying the feedback gain on the location of the pole in a zero-order feedback system

Consider a familiar example, the low-pass filter (with d.c. gain A , so $H(s) = A/(1 + sT)$). We now include this system in a feedback loop, by adding a constant feedback gain of $H(s) = k$ (Fig. 15). Let's see what happens when we vary k .

The transfer of the total system (response $R(s)$, divided by command $C(s)$) is:

$$H(s) = \frac{R(s)}{C(s)} = \frac{\frac{A}{sT+1}}{1 + \frac{Ak}{sT+1}} = \frac{A}{sT + 1 + Ak} = \frac{\frac{A}{1+Ak}}{1 + s \frac{T}{1+Ak}} \quad (38)$$

where we rewrote the transfer function such that we get it into the familiar form of $1/(s + a)$. Now use the pole-zero diagram to see what happens when k increases from zero. The pole of the transfer characteristic is found at $s = -(1 + Ak)/T$, which depends on the gain of the feedback loop!

When $k = 0$, the pole is at $-1/T$ (the regular LP system). As k increases, $-(1 + Ak)/T$ becomes more negative and the pole slides out along the negative real axis. In other words: the system becomes *faster* (shorter time constant). This path, shown as a thickened line, is the locus of all possible positions for the pole and this form of representation is also called the root locus.

It is a pictorial way of showing all possible behavioral patterns of a dynamical system and what to do with k to get a desired pattern. We will illustrate it for subsequent situations where it seems useful.

What it does not show is that the dc gain $A/(1+Ak)$ is also decreasing as k increases: as the bandwidth of the system increases (by leftward pole sliding), the gain decreases.

Question 19: Now consider the case where the feedback path of the negative feedback system in Fig. 15 is a pure delay, ΔT . The system is driven by a sinusoid, $x(t) = A \cdot \sin(\omega t)$, with frequency ω . When does the system become unstable?

2 June 30 (pm): The Saccadic System

2.1 General background

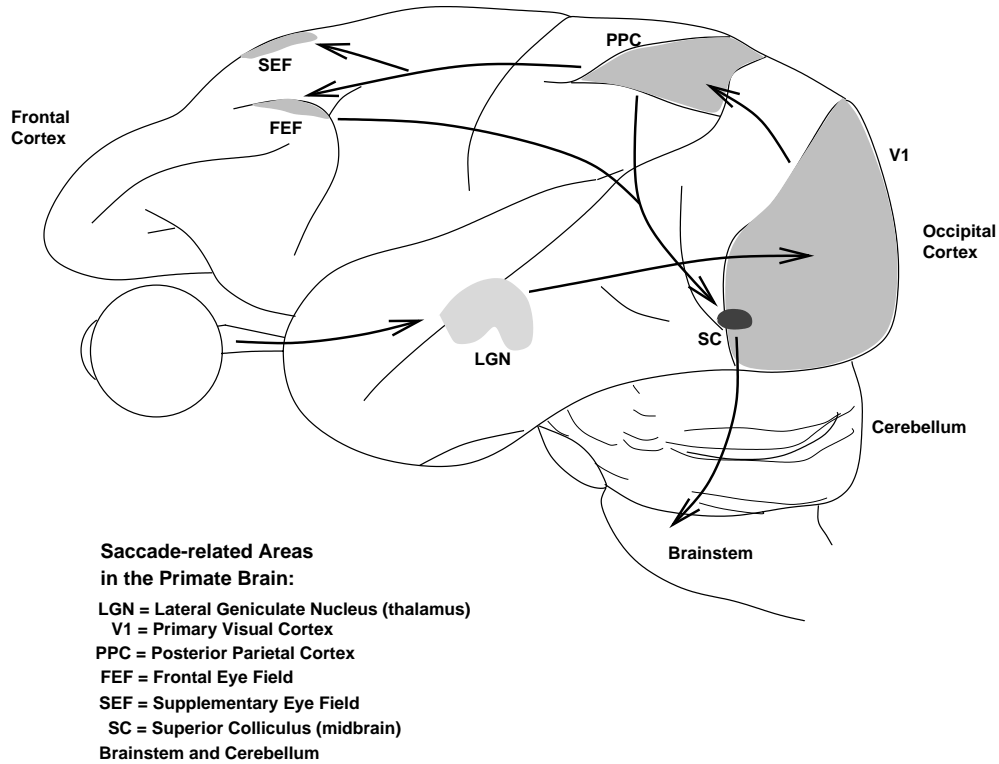


Fig. 16: Brain areas involved in saccade generation in monkey. Only the main cortical (V1, PPC, FEF and SEF), and a few subcortical structures (LGN and SC) are shown. The brainstem contains several saccade-related nuclei, which will be discussed later on. Arrows indicate main flow of visual information: from retina to LGN, first to V1. Then, via the parietal cortex (PPC) to the frontal areas (FEF and SEF). Both parietal and frontal cortex project to the SC (partly directly, partly via the Substantia Nigra), which in turn is connected to the brainstem.

In this section we deal with the **saccadic eye movement system**, the task of which is to redirect the line of sight (i.e., the fovea) as quickly and as accurately as possible to a newly-selected peripheral target. We make saccadic eye movements about 3 times/sec, whenever we are scanning our visual environment, or when we read.

Although this course will not deal with the **Cortex**, the cortical areas involved in saccades are shown in Fig. 16. The output from several cortical areas is transmitted to a small (about 3x3x2 mm) nucleus in the midbrain: the **Superior Colliculus**. From there, the command to make a saccadic eye movement is generated, and the coordinates of the eye movement vector are determined. There is quite some controversy in this research field, about whether neural activity in the colliculus only encodes the saccade vector, or whether that activity also relates to the actual instantaneous motor command. Other discussions revolve about the question of whether the colliculus could be the structure that closes the local feedback loop for saccades (see below). In this session we will assume, for simplicity, that the

colliculus encodes the coordinates of the saccade vector, and that the mean firing rate of the cells relates to mean eye velocity. The collicular command signals are relayed to the **Brainstem**, with its intricate circuit of interconnected nuclei, that is responsible for the execution of the actual eye movement. It is this final stage, which will be studied and discussed in this short course, where we take the point of view from systems analysis, and apply the different concepts discussed in the previous section.

All types of eye movements are eventually generated by the **oculomotor plant** (the eye ball ('globe'), surrounding tissues, and the extraocular muscles). For here it is important to accept that the plant effectively acts as an approximately *linear* system (we will deal with some of the details below), and that it can be characterized as a *low-pass filter* (i.e., the plant is 'overdamped'). The plant's time constant is (to first order) about 150 - 200 ms, which means that its impulse (and step) response (see Chapter 1) will have a duration of several hundreds of milliseconds. As we will see later, these properties are crucial for understanding the saccadic system.

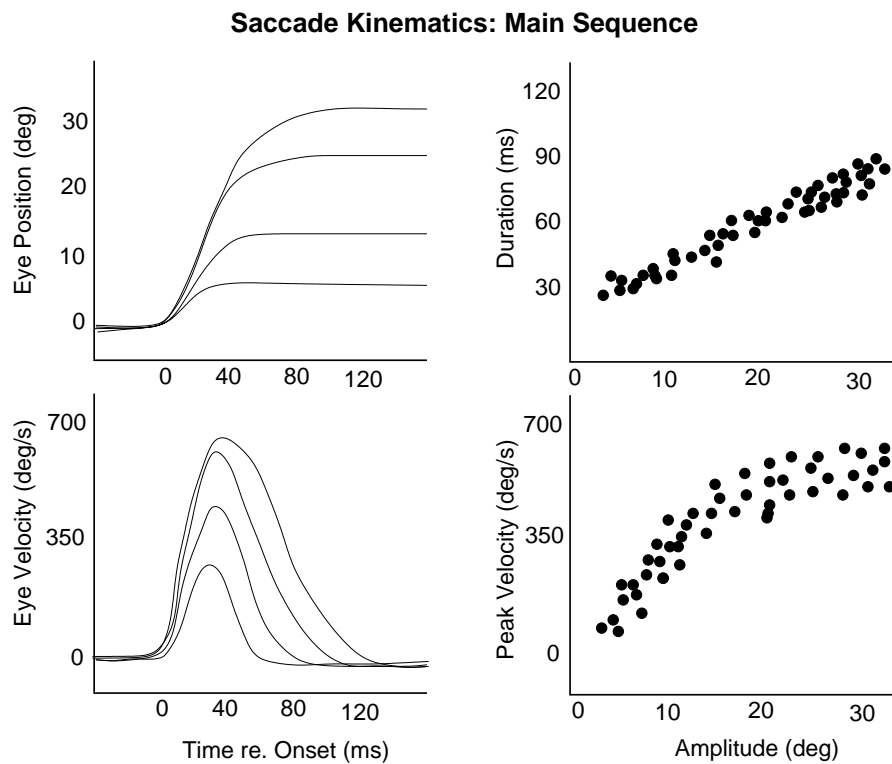


Fig. 17: Kinematics of saccadic eye movements of different amplitudes. Saccade duration increases as a straight-line with amplitude, whereas saccade peak velocity has a saturating relationship with amplitude. Also notice that the shape of the velocity profile changes with saccade amplitude.

2.2 Saccades.

Kinematic Properties of Saccadic Eye Movements:

Whenever the target is outside the current fixation area, the visuomotor system may program a saccadic

eye movement toward the peripheral stimulus.

Saccades are very rapid and accurate eye movements (in humans they can be as fast as 700 deg/s, but in rhesus monkeys even up to 1300 deg/s!). From the point of view of Systems Theory (Chapter 1), the input to the saccadic system may be regarded as a Step (sudden displacement of the target toward a new location). Thus, the saccade may be conceived of as the Step Response of the visuomotor system. When elicited by an unexpected target saccades have quite stereotyped kinematics (i.e. movement properties): the relations between saccade amplitude and saccade duration, and between amplitude and peak eye velocity are known as the ‘**Main Sequence**’ of saccadic eye movements. Fig. 17 shows these features for saccades. Interestingly, from the point of view from systems identification, already some very important conclusions can be drawn from the main-sequence behavior of saccades:

1. There can be no step-like motoneuron command.....

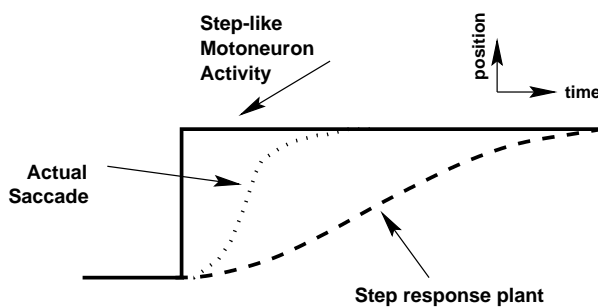


Fig. 18: The step response of the overdamped oculomotor plant (dashed line) is far too slow to explain real saccadic behavior (dotted line).

2.but a Pulse-Step motoneuron innervation is needed:

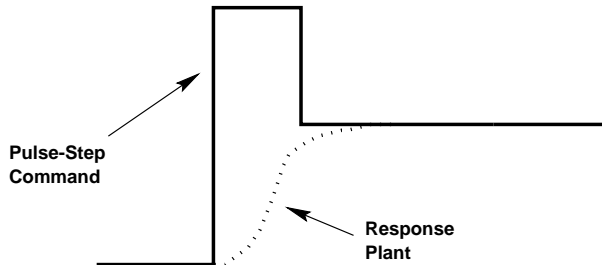


Fig. 19: A pulse-step response of the oculomotor plant (dotted line) may account for the kinematics of saccades.

3. The saccadic system is nonlinear!

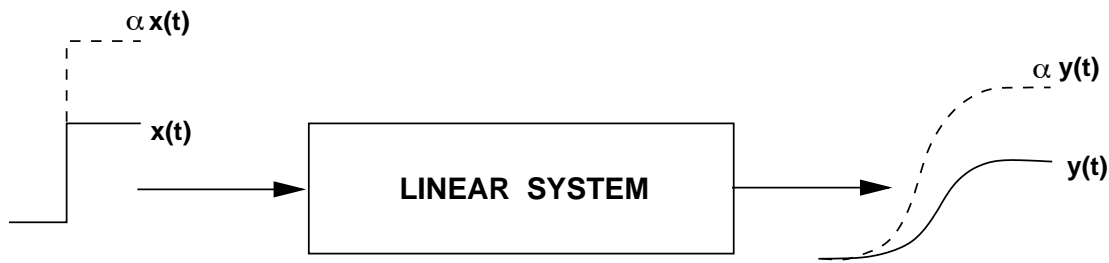


Fig. 20: Property of a linear system.

As indicated in Fig. 20 (and discussed at length in Chapter 1), linearity requires that whenever the input amplitude of a signal (e.g. the size of the target jump) is multiplied by an arbitrary factor, say a , the system scales its output by *the same* factor:

$$x_1(t) = a \cdot x(t) \Rightarrow y_1(t) = a \cdot y(t)$$

So, if the **input** to the saccadic system is considered to be a step-displacement of the target on the retina, one should conclude that because of the main-sequence properties of saccades (Fig. 17) the saccadic system as a whole acts like a nonlinear system.

Question 1 (all): Why can this conclusion be drawn? Draw (and motivate) the *expected* 'main sequence' of a (i.e. any!) linear system!

2.3 Neural Processes Underlying Saccade Generation.

1. **Target Selection.** From the virtually infinite number of potential visual (and auditory) targets, the CNS has to select the one for the saccade. Often, reflexes need to be avoided. Attentional (higher cortical) mechanisms play an important role in this selection process, which makes saccades also a hallmark system to study decision making!
2. Computation of the coordinates (i.e. direction and amplitude) of the eye movement. In this process, the saccadic system needs to account for not only the retinal error vector of the target (i.e. the angular distance of the target to the fovea), but also with the starting position of the eyes in the head, and with the orientation of the head on the neck (a problem that will be dealt with in this course on the second day!).
3. The initiation of the saccade, i.e. the actual decision, or 'trigger' to make the saccade and to 'disengage' the current fixation.

In a simple visual environment (e.g. a single target in an otherwise dark room) these three stages typically take about 200 ms to start the saccade. In more complex visual scenes the reaction time (or '*latency*') rapidly increases.

4. The actual control of the eye movement. It is assumed that the saccadic system continuously compares the actual eye movement to the desired eye movement, by means of an internal feedback loop, also called the *local feedback loop*. The properties of this latter stage will form the main topic of this exercise (see also below).

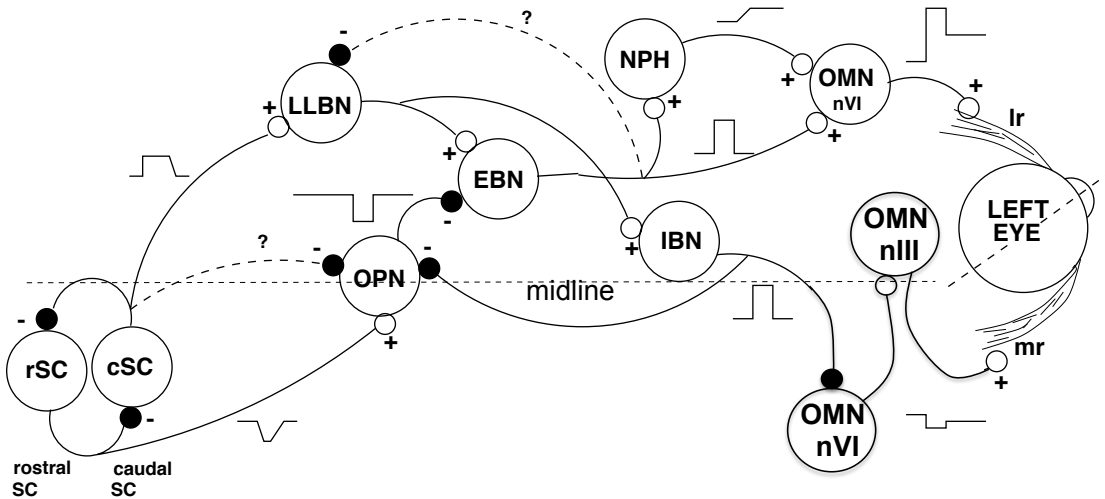


Fig. 21: A highly simplified scheme of the brainstem regions involved in the generation of horizontal (leftward) saccadic eye movements, shown for the left eye only. SC = superior colliculus (rostral zone and caudal part), LLBN = long-lead burst neurons, OPN = omni-pause neurons, EBN = short-lead excitatory burst neurons, NPH = tonic neurons, OMN = oculomotor neurons (nVI = abducens nucleus, nIII = oculomotor nucleus), IBN = inhibitory burst neurons. LR = lateral rectus muscle, MR = medial rectus muscle. Not all inhibitory interneurons are shown, for reasons of clarity.

2.4 The Saccadic Brainstem Circuitry

A number of different cell groups in the **brainstem** and **midbrain** have been extensively studied and much is known about their role in saccades. Here, we will limit the discussion to horizontal saccades (see Fig. 21), for which the relevant cell groups are (read this, learn it by heart, and you can have intelligent discussions with any neurologist!):

- Oculomotor neurons in the Abducens Nucleus (n.VI) and the third nucleus (n.III) (OMN)
- Tonic neurons (i.e. neurons firing at a d.c.-rate) in the Nucleus Prepositus Hypoglossi (NPH)
- Short-Lead Excitatory (EBN) and Inhibitory (IBN) Burst neurons in the paramedian pontine reticular formation (PPRF).
- Long-Lead Burst Neurons in the PPRF (LLBN)
- Omni-pause neurons in the Raphe Nucleus (OPN)

- Saccade-related burst neurons in the caudal Superior Colliculus (cSC)
- Fixation-related neurons in the rostral ('front') portion of the SC (rSC).

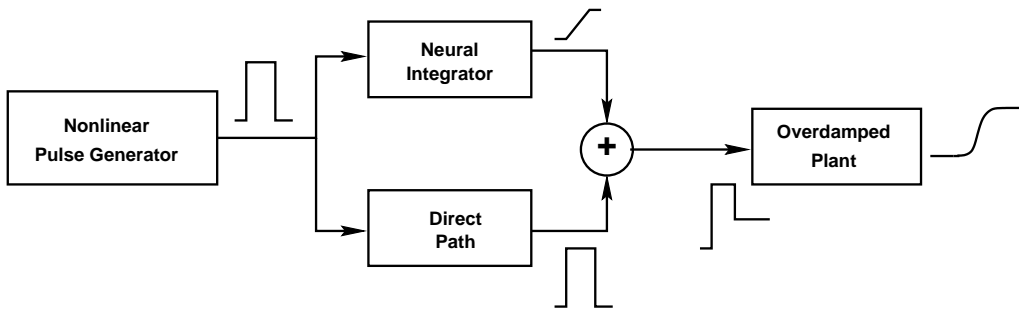


Fig. 22: The pulse-step generator of the saccadic system involves three stages (neural populations): pulse generation (PPRF), neural integration (NPH), and summation (OMN). See also the Computer exercises.

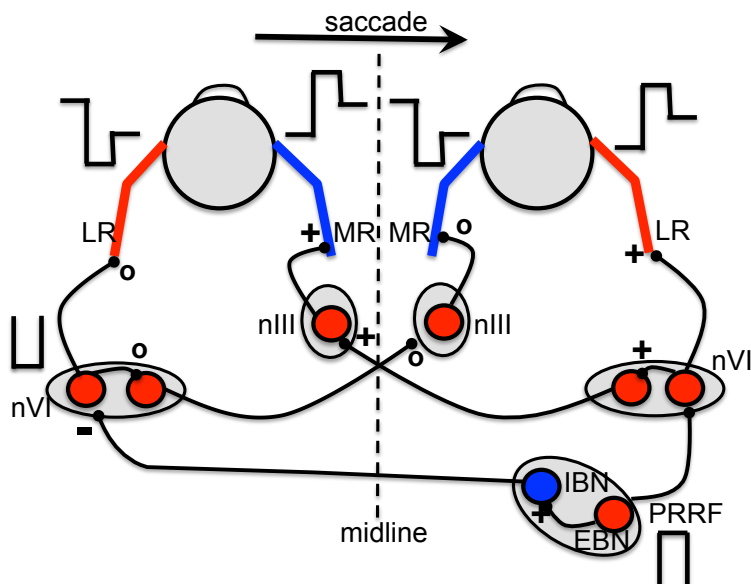


Fig. 23: Oculomotoneuron control of both eyes for a rightward horizontal saccade. Note the 'push-pull' organization of the different motoneuron pools (nVI and nIII; step NPH pathway omitted, for clarity). The EBNs in the PPRF on the right side send a Pulse to right LR and left MR. The right IBNs remove all innervation from the left LR/right MR.

The Oculomotoneurons (OMN) control a heavily-damped 'plant' (short-cut name for the ocular globe, the six extraocular muscles and surrounding tissues; see also below) with a so-called Pulse-Step command signal on the agonist muscle (see above), and often a complete cessation of activity on the antagonist (Note: a muscle's action is called *agonistic* when it pulls into the direction of net motion; it's called *antagonistic* when it pulls in the opposite direction.)

The **Pulse** component of this signal is needed to overcome the relatively strong viscous ('friction') forces that are especially prominent at the high saccade velocities (note that friction increases roughly quadratically with velocity). The **Step** component of the signal keeps the eye in its new peripheral orientation after the saccade has ended. It thus precisely compensates for the static elastic restoring forces of the eye muscles (which behave like mechanical 'springs').

Note, that the different neuronal pools that have to innervate the eye muscles, should be precisely coordinated. For example, horizontal eye movements are generated by either the Lateral Rectus muscle, which pulls each eye outwards, or the Medial Rectus muscle, which pulls each eye inwards. If **both** eyes are to move rightward, the LR of the right eye, and the MR of the left eye should be activated by a Pulse-Step signal, but at the same time, the MR of the right eye, and LR of the left eye should be silenced! Below, in Fig. 23, a more complete scheme is shown that does exactly that:

Question 2: What eye movement abnormalities result after damage of

- the *Abducens Nucleus* (nVI; i.e. the actual cells)?
- the *Abducens Nerve* (i.e. the output of the nucleus to the LR)?

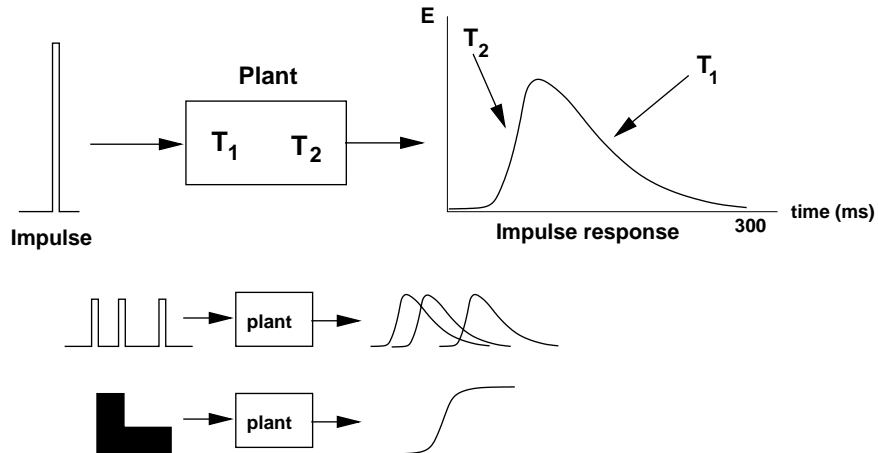


Fig. 24: Linear model of the plant is fully characterized by its impulse response. Conceptually, the impulse response is the (miniature) eye movement that would result in response to a single spike at its input. Due to the **superposition principle** resulting from linearity, the plant's response to a burst of spikes is the linear sum all single-spike impulse responses.

Long-Lead and Short-Lead Burst Neurons are a crucial part of the central saccade generator in the brainstem. Lesions ('=beschadiging') in the paramedian pontine reticular formation, where these neurons are found, lead to a complete abolition of all horizontal saccades toward the side ipsilateral to (i.e. to the same side of) the lesion. It is generally held that these neurons are crucial for the generation of both the pulse and the step components of the motoneuron command for both eyes. The antagonist muscle relaxes due to the action of inhibitory burst neurons (IBNs; Fig. 21). Quantitative analysis of the activity of these burst neurons (especially in the EBNs and IBNs) shows a strong relation with eye

velocity, and it is thought that these firing patterns underly the nonlinearity in saccade kinematics (see above). This relation is less tight in the LLBNs.

The **tonically active neurons** in the NPH are supposed to embody the **neural integrator** that generates an **eye-position** related signal (the 'step') from the velocity burst of the EBNs/IBNs.

The 'plant' is highly over-damped, but **linear** for a considerable range of movements. It is usually modeled as a second-order linear system. This means two things:

- (i) that its input-output relation can be described by a second-order linear differential equation, and
- (ii) that its **impulse response** can be characterized by two time constants.

The long time constant (T_1 about 150 ms) is mainly determined by the elastic properties of the muscles, the short time constant (T_2 about 12 ms) is related to the plant's viscosity.

The **Impulse response** of the plant, $h(\tau)$, is given by the following equation:

$$h(\tau) = \frac{1}{T_1 - T_2} \left[e^{-\frac{\tau}{T_2}} - e^{-\frac{\tau}{T_1}} \right] \quad (48)$$

Question 3 (all):

Make a graph of $h(\tau)$, and determine the location of its maximum.

By assuming that in certain neurological diseases the oculomotor plant itself remains unaffected, many typical oculomotor problems associated with horizontal saccades can be diagnosed.

The **OmniPauseNeurons** (OPN) are crucially involved in the **initiation** of the saccade. Their firing follows a reverse pattern as that of burst neurons: they are active during fixation, and silent during the saccade. It is therefore thought that EBNs and OPNs form mutually inhibitory connections.

As has been extensively documented by a number of studies, cells in the caudal zone of the **Superior Colliculus** are arranged in a so-called **Motor Map**. Each saccade vector appears to be associated with a specific group of SC cells. Such a localized group of cells sends a burst of spikes to the brainstem saccade generator. Burst onset is tightly coupled to saccade onset, but only loosely related to saccade kinematics. In fact, the burst properties of different SC sites appear to be very similar across the entire motor map. In models of the SC it is therefore assumed that large and small saccades are encoded by the synaptic connectivity of the different groups of SC cells, rather than by their specific firing rates. Cells in the rostral pole of the SC having firing properties that resemble those of the OPNs, to which they make direct connections. It is therefore assumed that these rostral cells play a role in fixation by exciting the OPNs.

Question 4 (all): Assign, in Fig. 25, the correct neural pathology to its associated saccade abnormality.

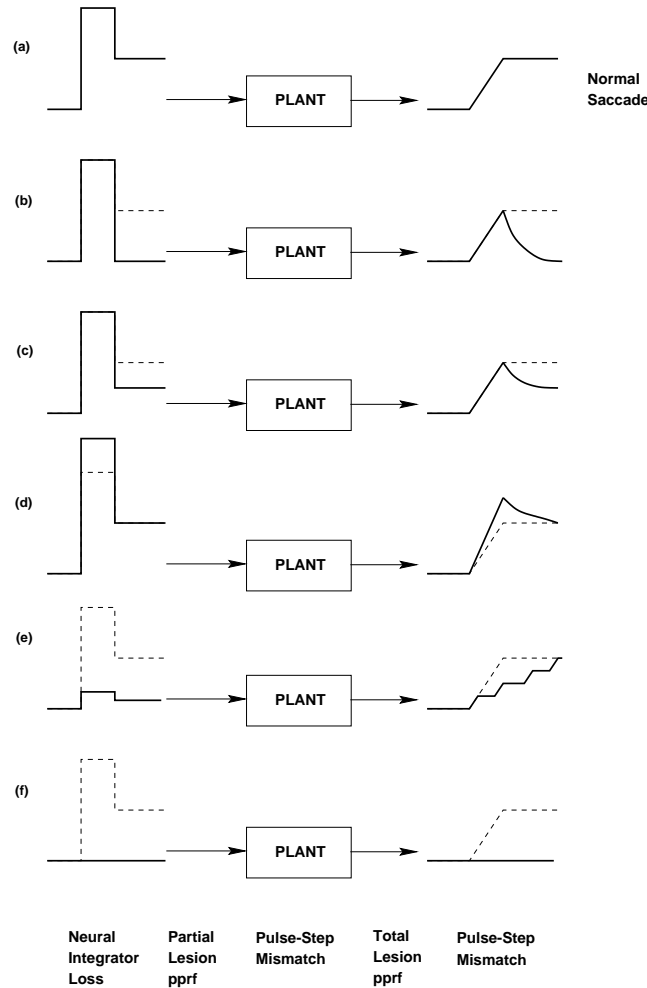


Fig. 25: Pathologies in different parts of the pulse-step generator cause specific abnormalities in saccade behavior.

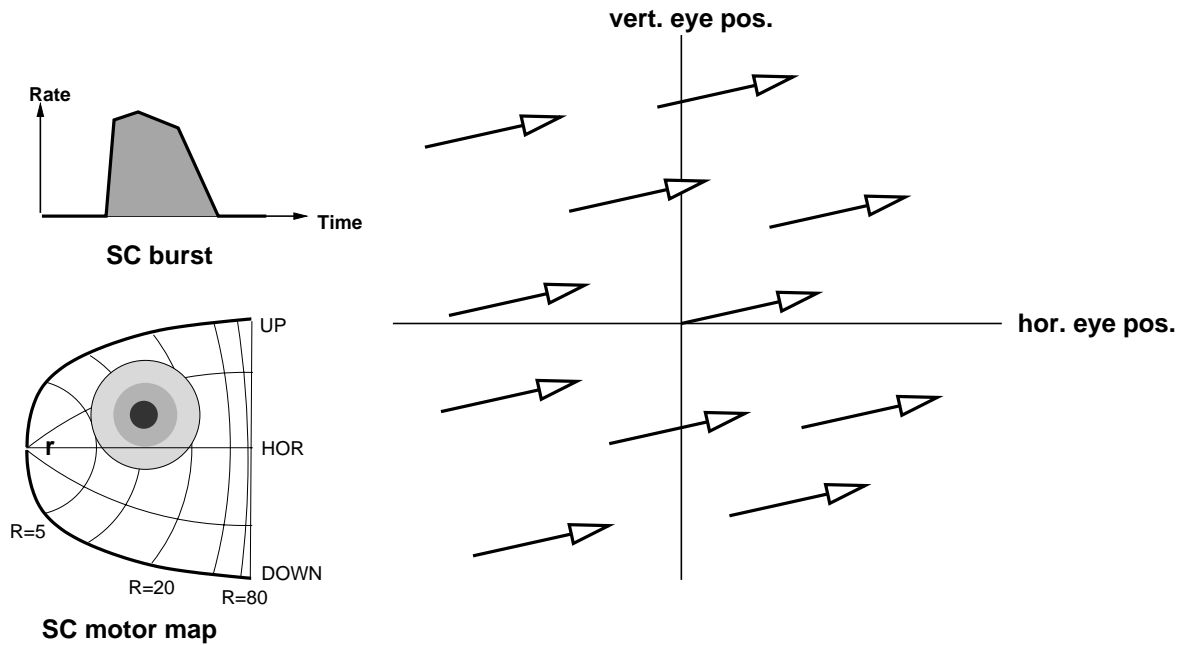


Fig. 26: A local population of cells in the caudal SC motor map (circular, grey-shaded area) sends a (roughly fixed) burst of spikes (top-left figure) to the brainstem. A given population encodes a fixed eye displacement vector, irrespective of initial eye position (right figure). Thus, for all saccades shown, the same population of cells will be equally recruited. Different saccade displacements are encoded by different populations in the map. r =rostral fixation zone.

2.5 Scudder's Model of the Saccadic System.

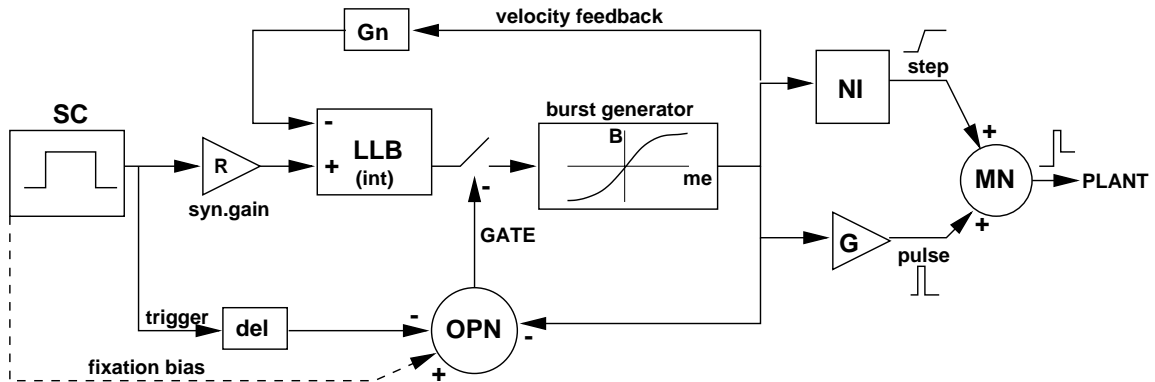


Fig. 27: Scudder's (JNP, 1988) saccade model that includes the Superior Colliculus (SC), Long-Lead Burst neurons (LLB) and the burst generator in the brainstem. The saccade Gate (OPN firing rate) is controlled by the rostral Superior Colliculus: its fixation-related activity (and thus EBN inhibition) prevents saccade initiation. The saccade trigger (which inhibits the OPNs, thus releasing the EBNs) is given when the saccade-related caudal SC cells in the motor map exceed a threshold.

In this part of our Introductory course, we discuss and describe an interesting conceptual saccade-control model. This theoretical model is based on a vast amount of experimental data (obtained from electrophysiology in trained monkeys and cats, and from data such as in Fig. 17), and was proposed by Charles Scudder in 1988 (Journal of Neurophysiology).

Due to the relative simplicity of this model, and to its close correspondence to realistic midbrain-brainstem neurophysiology, it is a nice model to illustrate some of the basic concepts that have been dominating the oculomotor field during the last decades. The model is also a fine example of the power of computational modeling with Neural Networks and System's Theory and of their potential to probe and understand neurobiological systems and pathologies.

The model provides a detailed explanation of the two final steps in the saccade generation process (see above): the **initiation** and the **execution** of a saccadic eye movement. Note, that the model is *not* intended to mimic cognitive behavior, or target selection mechanisms (like the Countermanding Paradigm, Antisaccade Paradigm, or decision making). Everything considered 'upstream' from the Superior Colliculus (Basal Ganglia and Cortex) is beyond the scope of the model.

However, the model *does* provide valuable insights into several properties of the saccadic system (see above), and of the connectivities and functional role of the midbrain Superior Colliculus and of several crucial brainstem nuclei.

It is also very useful for the diagnosis of certain neurological pathologies that appear to have their effects on saccade generation mechanisms (such as brainstem palsies, Parkinson's disease, Huntington's disease, etc.). Several of these aspects may be studied by means of the computer simulation programs.

The model is based on a number of assumptions and experimental findings:

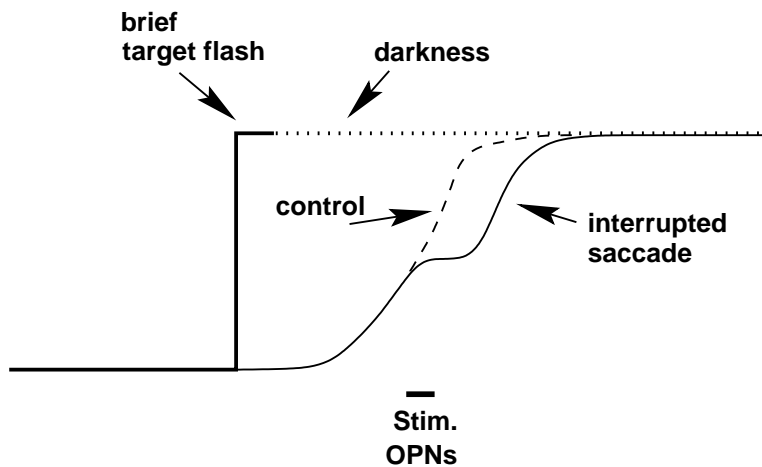


Fig. 28: Evidence for local feedback in the saccadic system. Brief stimulation of the OPNs causes the eye to stop in midflight. However, in the absence of visual feedback, the resuming eye movement reaches the extinguished target position.

1. Saccades are controlled by an **internal, local feedback loop**. In Scudder's model, the feedback loop carries the *velocity* output from the Inhibitory Burst Neurons. Below, we will discuss the potential benefits of feedback into somewhat more detail.

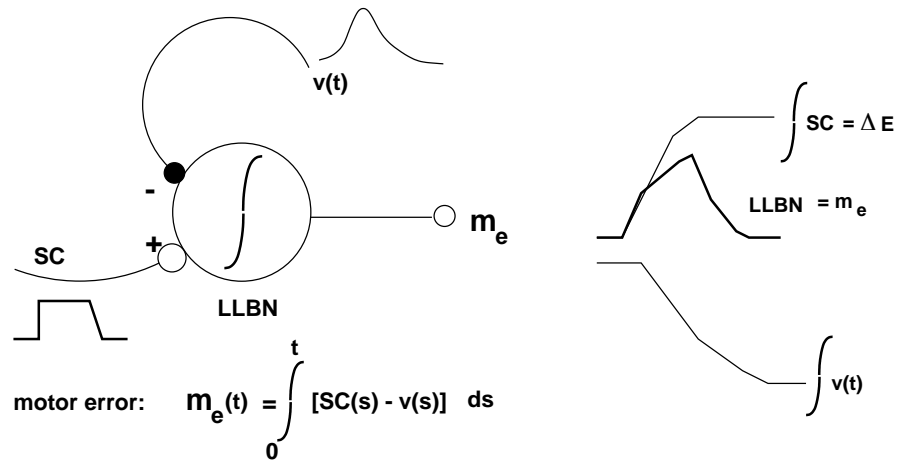


Fig. 29: The LLBNs integrate the ongoing difference between the SC burst and the feedback velocity signal from the EBNs. Note, that according to the saccade model, the SC firing rate encodes desired eye velocity, whereas the number of spikes in the SC burst encodes the desired eye displacement, ΔE . The output of the LLBNs is instantaneous eye motor error, $m_e(t)$.

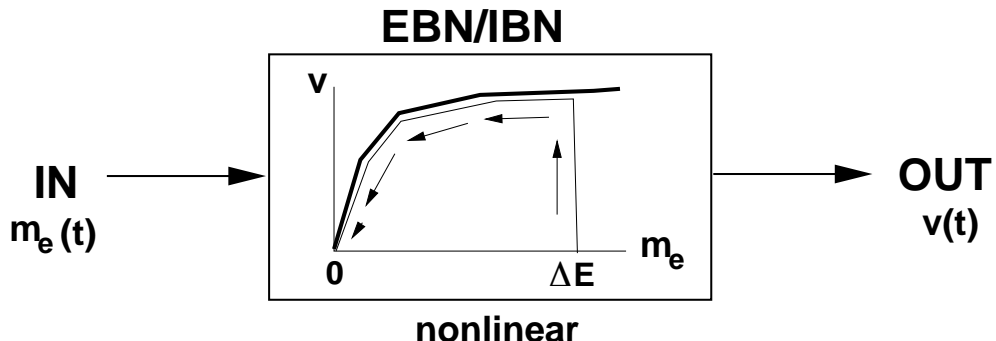


Fig. 30: The EBN's and IBN's embody the saccadic pulse generator. It transforms eye motor error into an eye velocity command: the larger eye motor error, the higher the eye velocity. As motor error falls to zero (due to the internal feedback loop), eye velocity goes to zero too. Note that the transformation is a saturating nonlinearity, that accounts for the Main Sequence of Fig. 17.

2. The **Long-lead Burst** cells compare the saccadic command from the Superior Colliculus, with the neural (internal feedback) estimate of the actual eye movement. The difference between these signals is time-integrated by the LLBNs. Their output is a neural estimate of the **current motor error**, m_e . The motor error is the distance the eye still is to go to reach the target. This signal drives the two kinds of short-lead burst cells (EBNs and IBNs).

3. The **Burst Neurons** have a nonlinear (saturating) input-output characteristic (Fig. 30). In the saccade model, the relation between current motor error and the eye-velocity (pulse) command is given by:

$$v(t) = V_0 \cdot \left[1 - e^{-\frac{m_e(t)}{e_0}} \right] \quad (49)$$

where V_0 is the **asymptote**, and e_0 is the **angular constant** of the nonlinearity.

3 June 30 (pm): The Computer Models

In the afternoon computer exercises we will investigate the main properties of Scudder's saccade model by means of numerical simulations with Simulink. By interactively changing the parameters in the model, we will gain a further understanding of

- some elementary concepts of the systems-theoretical approach: linearity, nonlinearity, feedback,
- the role of different brainstem nuclei in saccade generation.
- the effect on saccades of specific brainstem lesions.

3.1 Part 1: PulseStep.mdl

To gain more insight into the concept of **Pulse-Step Generation**, and also to get more acquainted with the ideas behind **Linear System's Theory**, a simple model of the so-called 'Final Common Pathway' of the oculomotor system is also available under Simulink as file:

`pulsestep.mdl`

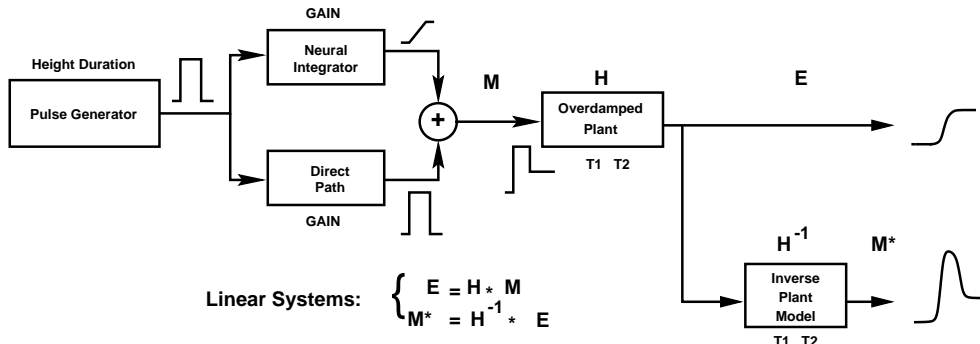


Fig. 31: Model of the Final Common Pathway of the Oculomotor System. For saccades, this embodies the Pulse-Step Generator. The output of this pathway (i.e. eye position) is subsequently fed through an Inverse Model of the Plant, to enable a reconstruction of the motoneuron signal (see also Figs. 18 and 19).

This simulation model (compare it to the final part of the saccade model), allows you to interactively set parameters of

- The *saccadic burst* from the EBNs/IBNs (this is simply modeled as a pulse, having a height, **P**, and duration **D**).
- The *neural integrator*: setting its gain to zero mimics total loss of the integrator, whereas a gain of one means normal operation.
- The *direct path*: feeds the pulse directly to the oculomotor neurons. When its gain is set to zero, you actually simulate the effect of a *Step* input to the OMNs.

- The *Plant*, with its two time constants, T_1 and T_2 .

Model parameters of PulseStep.mdl:

Stage	Symbol	Meaning	Range	Default	Unit
Burst Generator	P	Pulse height	[0 - 1000]	700	Hz
	D	Pulse duration	[0 - 0.20]	0.06	sec
Neural Integrator	G	Gain	[0 - 1.0]	1.0	-
Direct Path	k	Gain	[0 - 0.5]	0.15	-
Plant	T_1	Long Time Constant	[0.05 - 0.30]	0.15	sec
	T_2	Short Time Constant	[0 - 0.03]	0.012	sec

Exercise 2.1: Parameters.

First play with this model by changing the Burst parameters, the Neural Integrator gain, and the Plant time constants. Note what happens with each change in parameters. How do you determine the amplitude of a saccade?

Verify that the model is linear.

Excercise 2.2: Determine the Step response of the oculomotor plant. What do you see?

Excercise 2.3: How would you set the model parameters, if you want to simulate the impulse response of the plant? Verify your proposal.

Exercise 2.4: Pulse-Step mismatch - I.

Start with the default model parameters. We concentrate on 20 deg saccades only (How would you ensure a 20 deg saccade?). Now vary only the strength of the Forward Gain in the pulstep model. Describe the effect of these changes on the saccade. Explain. Do the same effects also occur for saccades of different amplitudes?

Exercise 2.5: Pulse-Step mismatch - II.

Again keep your default parameter set. Now only vary the long time constant of the plant, T_1 . Describe the effects on the saccades, and explain. What do you conclude when you combine these effects with the previous exercise? Test your hypothesis by introducing large variations in both parameters, such that **NO** effect results on the saccades. Does your parameter choice depend on the saccade amplitude?

Exercise 2.6: The Neural Position Integrator.

By changing the gain of the Neural Integrator between 0 and 1, you may study the effects of NI lesions on the saccades. Describe these effects (other parameters default). Also change the long time constant of the plant. Explain your results.

Excercise 2.7: Pulse-Step reconstruction - I:

An additional feature of this simple simulation model is the possibility to *reconstruct* the actual net motoneuron input to the plant, on the basis of the (simulated) eye position signal. To that means, an inverse model of the plant is incorporated (see Fig. 33). Simulate the model with its default parameter set and note the (quite reasonable) resemblance between the reconstructed OMN input and the original Pulse-Step input.

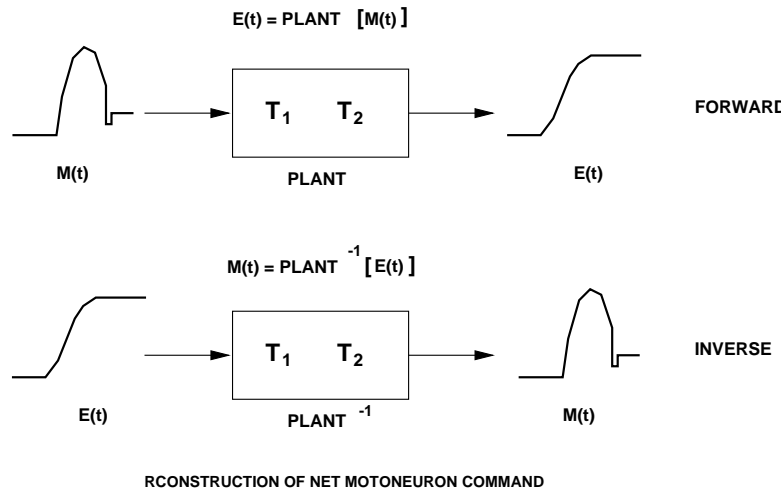


Fig. 32: By virtue of the plant's linearity, it is possible to reconstruct an estimate of its net neural pulse-step control signal from the measured eye movement, $E(t)$.

Question: Explain how the inverse simulation is achieved (Hint: When you open the box, ('Look under Mask'), you'll notice that feedback is used, but why does it do the trick?). Any idea why actual pulse-step and reconstructed pulse-step are not exactly identical?

3.2 Part 2: Saccade.mdl

Exercise 3.1: Run the Saccade model with its default parameter set (these are already set, but see Table, below for an example) for different saccade amplitudes. The different amplitudes are obtained by changing the value of the **syn.gain** box (= 'synaptic gain'), which represents the connection strength of a particular SC site to the saccade generator.

Parameters of Saccade.mdl:

Stage	Symbol	Meaning	Range	Default	Unit
SC Burst	FR	Burst height	[0 - 1000]	800	Hz
	D	Burst duration	[0 - 0.20]	50	msec
Syn. Gain	R	Connection strength from SC to Brainstem	[0.1 - 1.5]	0.5	-
Burst Generator	Bmax	Pulse height	[0 - 1000]	700	deg/sec
	A0	Angular constant	[1 - 100]	7	deg
OPNs	Bias	Firing rate of OPNs during fixation	[50-500]	80	Hz
Neural Integrator	G	Gain	[0 - 1.0]	1.0	-
Feedback Path	Gn	Feedback Gain	[0 - 5]	1.0	-
Direct Path	k	Forward Gain	[0 - 0.5]	0.15	-
Plant	T ₁	Long Time Constant	[0.05 - 0.30]	0.15	sec
	T ₂	Short Time Constant	[0 - 0.03]	0.020	sec

Exercise 3.2: Obtain the Main Sequence of normal saccades (see e.g. Fig. 17). Ensure that the parameters of the PSG, the BG and the SC, have their default values (see Table). Then, vary the parameters of the BG (saturation level and angular constant, Fig. 29), to verify the effect on the main sequence. Make a **graph** of the different main sequences (with BG parameters). Obtain **amplitude** and **peak velocity** of saccades by reading out the displays. Saccade **duration** may be taken as the time interval where eye velocity exceeds about 10% of its peak velocity.

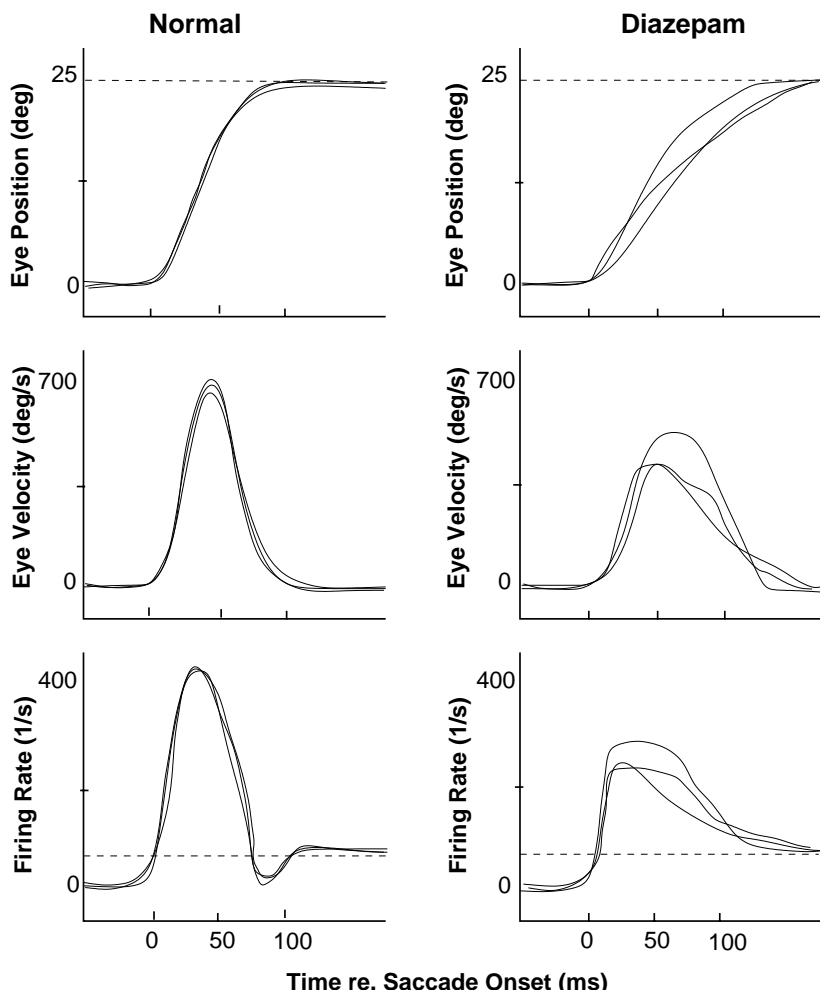


Fig. 33: Effect of an intravenous injection of Diazepam (Valium) on human saccades toward flashed targets: although the Valium saccades (right) are still quite accurate, their kinematics are much more variable and slower than normal responses (left). Note also the differences in the reconstructed Pulse-Step signals (bottom). (After: Van Opstal *et al.*, *Vision Res.*, 1985)

Exercise 3.3: Fig. 33 shows the effect of 7 mg Valium on human saccades. Explain the (average) experimental results with the saccade model, if we assume that the benzodiazepines have no effect on the mechanical properties of the plant, but only affect the CNS. Support your explanation with simulations.

Exercise 3.4: Influence of the feedback gain.

Start with the default parameters, and concentrate on 20 deg amplitude saccades. Vary the gain in the feedback loop between zero and 2.0. Try to explain the resulting effects.

Exercise 3.5: The OPNs.

Keep the amplitude of the saccade fixed at e.g. 20 deg. Now only change the timing of the OPNs, by changing the *delay* of the SC-trigger burst.

Describe the effect on the LLBN burst of these changes, and on the kinematics of the resulting saccades. Explain your observations.

Exercise 3.6: The SC burst.

Keep the amplitude of the saccade fixed at e.g. 20 deg. Now only change the parameters of the SC burst (everything else being default). First ensure, however, that the total number of spikes in the burst (i.e. the integral of the pulse: width \times height) remains fixed. Describe the effects on the saccades, and explain.

Subsequently, drop the demand on the number of spikes and explain the effect of either a change in burst intensity and/or a change in burst duration.

4 Scudder revisited: common source and superior colliculus

4.1 Two-dimensional eye-movements: the Common Source Model

The vertical saccadic pulse-step generator in the brainstem consists of burst cells in the medial longitudinal fasciculus (MLF), and the neural integrator resides in the nucleus of Cajal (NC). Neurophysiology has revealed that cells in this pulse-step generator are tuned to movements in the vertical/torsional plane. For simplicity's sake (Stefan, sorry!), and to avoid the additional complexities of noncommutative rotational kinematics, we will ignore the torsional dimension, and consider eye movements with horizontal and/or vertical components only.

The horizontal and vertical saccade burst generators receive a common input command from the SC, that is thought to represent a desired vectorial displacement of the eye (Δe_d) relative to the initial eye position (see also below). As will be described in great detail later, the SC signal is spatially encoded in a topographic motor map, in the sense that neighbouring recruited regions in the map encode similar saccade vectors by their *location* within the map, rather than by the intensity of the neural activity. The transformation of this *vectorial* eye-movement signal into the appropriate activation patterns of the eye muscles, is known in the literature as the *spatial-temporal* transformation stage, and involves two different processes:

- (a) **Vector decomposition (VD)** into horizontal and vertical saccade components.
- (b) **Pulse generation (PG)** of dynamic motor error, $m(t)$, into an eye velocity command, $\dot{e}(t)$.

The VD stage is *linear*: $\Delta H = R \cdot \cos \Phi$, $\Delta V = R \cdot \sin \Phi$, as it scales linearly with the saccade amplitude.

However, the PG stage is typically assumed to be nonlinear, since it is described by a saturating function that accounts for the observed saccade kinematics: $\dot{e} = a[1 - \exp(-b \cdot m)]$, see above, Fig. 17. As a result, the order in which these two processes are implemented in the system matters (it is a non-commutative operation):

$$VD \circ PG \neq PG \circ VD$$

(In the next chapter, however, we will challenge the necessity of a nonlinearity in the brainstem).

Study of oblique saccades has revealed that both saccade components are tightly synchronized and coupled, such that approximately *straight* saccades are elicited in all directions. In the so-called '*common source scheme*' a vectorial burst generator issues a vectorially-encoded velocity pulse command (PG), that is subsequently decomposed (VD) into the respective horizontal and vertical velocity components (see Exercise 4.1).

4.2 Neural mapping principles of the visual input

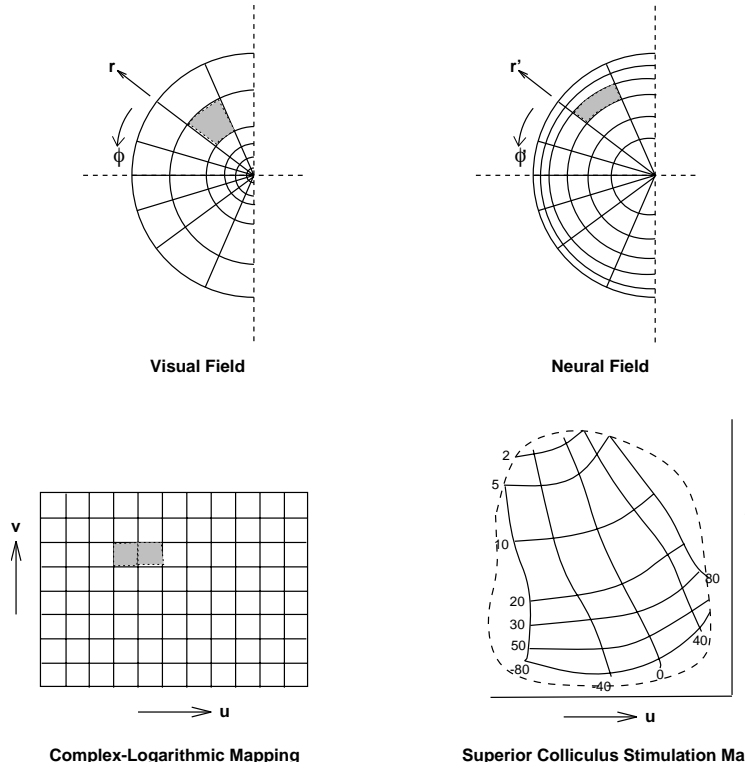


Fig. 34: *Mappings of visual space onto neural space, incorporating the experimental fact that equal numbers of retinal cells generate a visual receptive field, irrespective of eccentricity, but that cell density decreases with eccentricity according to an inverse square law. Note that the neural mappings preserve area and local angles (conformal maps). Top Left: visual space. Top Right: mapping that preserves radians and circles. Bottom Left: Complex-log mapping does not preserve radians and circles (see text). Bottom Right: Electrical stimulation of the SC yields saccade vectors whose directions and amplitudes only depend on the site of stimulation (drawn as iso-amplitude and iso-direction lines). Note that the stimulation map resembles the complex-log map quite well.*

The following organization principles apply to the retinal input:

- [1] Cell density in the retina, d , decreases with increasing eccentricity from the fovea, r : $d = d(r)$.
- [2] The sensitivity of a sensory neuron is described by its *Receptive Field*. In the retina, receptive fields of output ganglion cells are circular-symmetric. Experimental data have shown that the radius, σ , is proportional to distance, r , of the cell from the fovea: $\sigma \propto r$
- [3] The total number of stimulated retinal cells, $N = \pi \cdot \sigma^2(r) \cdot d(r)$ (with $d(r)$ cell density), is roughly constant (about $N=35$): a visual stimulus matched to receptive field size, always influences the *same number* of retinal cells. Thus, cell density decreases as: $d(r) \sim 1/r^2$

So how is the visual field mapped into the neural space of, let's say, the primary visual cortex?

Suppose that ΔA is a small area in the visual field, that is represented by ΔN retinal (ganglion) cells. We know that the receptive field area, $A = \pi\sigma^2$, is represented by *equal* numbers of retinal ganglion

cells, N , irrespective of r .

Thus, a relative change in receptive field size results in an equal change in relative cell numbers. Therefore, the neural mapping should satisfy the following constraint:

$$\frac{\Delta A}{A} = \frac{\Delta N}{N} \quad (50)$$

A function that fulfills the condition of Eq. 50 is given by the *complex-logarithmic function*, which is defined by:

$$\begin{aligned} \mathbf{z} &\rightarrow \mathbf{w} = \ln(\mathbf{z}) \\ \text{where } \mathbf{z} &= x + i \cdot y = r \cdot \exp(i \cdot \phi) \\ \text{and } \mathbf{w} &= u + i \cdot v = r' \cdot \exp(i \cdot \phi') \end{aligned} \quad (51)$$

In other words, the neural mapping is of the form:

$$\mathbf{w} = \mathbf{B} \cdot \ln \mathbf{z}$$

i.e.

$$u = B \ln \left(\sqrt{x^2 + y^2} \right) = B \ln(r) \quad \text{and} \quad v = B \cdot \arctan \left(\frac{y}{x} \right) = B \cdot \phi$$

(r and ϕ in radians). B is termed the neural ‘*magnification factor*’, and indicates the amount of neural space (in mm) per radian angular change in the retina. A function of this type has been proposed to underlie the neural mapping from visual retinal space into visual cortical space.

Note the singularity of this function at $r = 0$, and note also the ‘*forbidden regions*’ given by $|v| > B \cdot \pi/2$. Thus, the entire 2D visual world (either in cartesian or in polar coordinates) is mapped onto a narrow, logarithmic ‘*strip*’ of neural tissue.

You may verify that radians ($\phi = \text{constant}$) are transformed into parallel horizontal lines, whereas circles ($r = \text{constant}$) transform into parallel vertical lines (see Fig. 42). For visual cortex, experiments have yielded a magnification factor of 1.4 mm/rad for both u and v coordinates (i.e. an *isotropic* mapping).

4.3 Sensorimotor mapping in the Superior Colliculus

For the midbrain Superior Colliculus, the afferent (= input, sensory) mapping function appears to be only slightly different than the visual cortical complex-log map described above. First, the singularity at $r = 0$ is resolved by introducing the shift vector $\mathbf{A} = (A, 0)$, which appears to be quantitatively different from the one proposed for the visual cortex (see also Exercise 4.2). Second, the mapping appears to be slightly *anisotropic*.

The experiment that led to a quantitative description of this mapping function is shown in Fig. 42 (down and right). It is a remarkable fact that by applying a small electrical pulsatile current (threshold about $10\mu\text{A}$) to a micro-electrode that is positioned within the SC, it is possible to elicit a perfectly normal saccadic eye movement. Neither the stimulation intensity, nor changes in the pulse-frequency have any influence on the ensuing saccade. Only by stimulating at different *sites* within the SC is it possible to yield different saccade vectors: the amplitude (R) and direction (Φ) of the vectors then appear to

change smoothly as a function of the neural coordinates, (u, v) (mm). Fig. 42 shows the iso-amplitude ($R = [2, 5, 10, \dots, 50]$ deg) and iso-direction ($\Phi = [-80, -40, 0, 40, 80]$ deg) lines of elicited saccades, superimposed on the cartesian (u, v) -plane. Note that the resulting *experimental map* (the so-called *motor map* of the SC) has much in common with the *mathematical* complex-logarithmic mapping function.

It was therefore proposed to describe the experimental data by the following function:

$$\mathbf{w} = \mathbf{B} \cdot \ln \left(\frac{\mathbf{z} + \mathbf{A}}{\mathbf{A}} \right) \quad (52)$$

where $\mathbf{B} \equiv (B_u, B_v)$ are slightly different magnification factors, for the horizontal and vertical domain in cartesian neural space, respectively, and $\mathbf{A} = (A, 0)$ (in deg) prevents the singularity at $r = 0$. A nonlinear regression on the electrical stimulation data of Fig. 1 (bottom right) has yielded as best-fit parameters for the monkey SC motor map: $B_u = 1.4$ mm, and $B_v = 1.8$ mm/rad, and $A = 3$ deg. Thus, written in a slightly different way:

$$\begin{cases} u = B_u \cdot \ln \left(\sqrt{R^2 + 2A \cdot R \cdot \cos(\phi) + A^2} / A \right) \\ v = B_v \cdot \arctan \left([R \cdot \sin(\phi)] / [R \cdot \cos(\phi) + A] \right) \end{cases} \quad (53)$$

Properties of the map:

- [1] It is a *conformal* mapping, i.e. that angles (in receptor space) are invariant under the transformation and surface is preserved.
- [2] It is an *inhomogeneous* mapping (expansion for small R (small eye movements to targets near the fovea), and a compression for large R (large saccades)).
- [3] It is a slightly *anisotropic* mapping, i.e. no conservation of *shape* under the transformation (a square becomes an elongated rectangle) (see Exercise 4.4).

4.3.1 The SC movement field

When the saccadic system prepares a saccadic eye movement, the correct site in the motor map of the SC is selected to activate the local neurons at that site. The stimulation experiment (e.g., Fig. 26) showed that, indeed, if a local population of such neurons is activated, a reliable saccade vector signal is sent to the brainstem. Now, what do recordings from these neurons tell us under normal conditions? For this, we have to introduce the concept of a *movement field*: if one records from a SC neuron, the cell is active *only* when the saccade vector belongs to a restricted range of amplitudes and directions. This range of saccade vectors is called the cell's movement field (cf. receptive field for sensory neurons). The movement fields have a number of properties:

First, the SC movement field is *not* rotationally-symmetric, but appears to be markedly *skewed* along the amplitude dimension (see e.g. Fig. 35, bottom right), whereas it has roughly a gaussian shape along the direction coordinate.

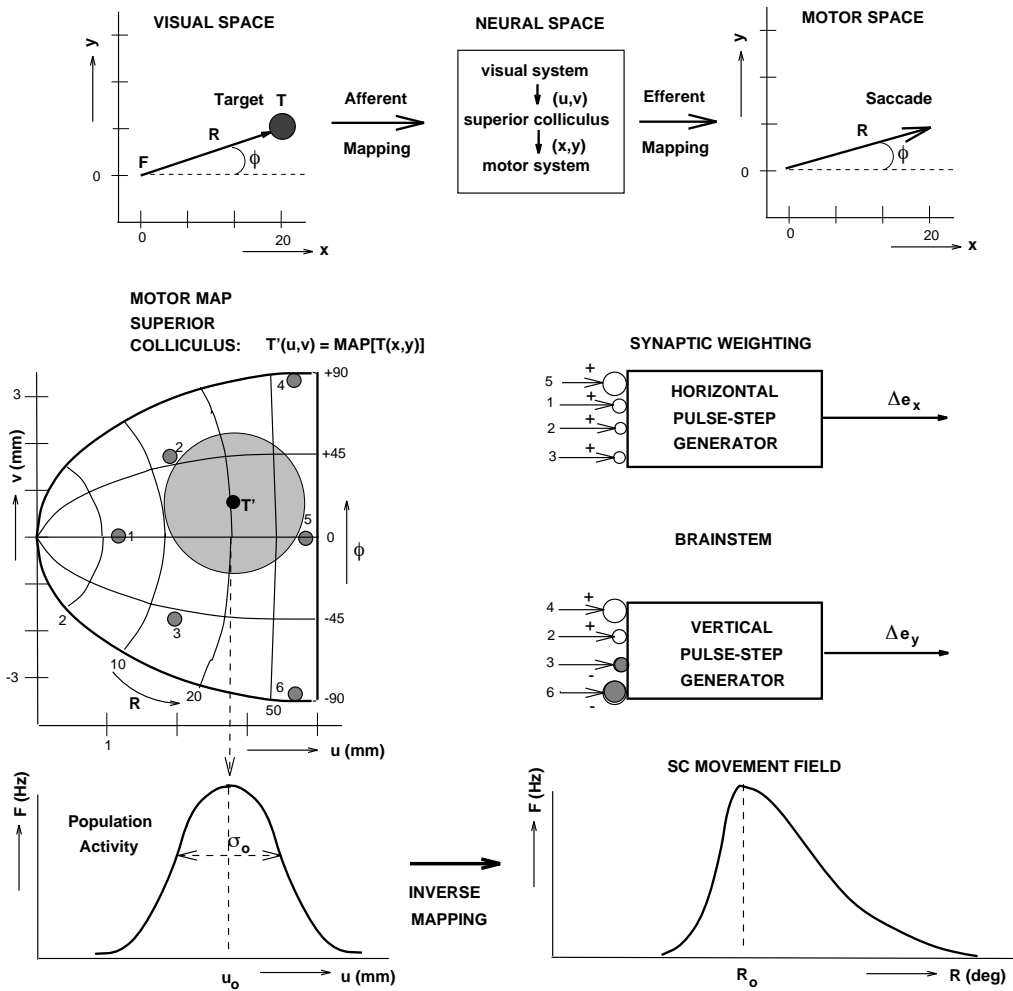


Fig. 35: Conceptual model of the mappings that take place between the early visual stage of the retina, and the final motor stage in the brainstem (top). Center: Complex-logarithmic motor map of the Superior Colliculus. (u, v) anatomical coordinates; (R, ϕ) polar coordinates of saccade vector corresponding to site (u, v) through Eq. 53. Lines superimposed on the motor map are iso-amplitude (run roughly vertical) and iso-direction (roughly horizontal) curves. The large filled circle represents the collicular gaussian population profile, when recruited for a saccade 20 deg to the right and slightly upward. Small filled circles are represent the locations of individual cells in the motor map. The strength and sign of their synaptic efferent connections to the horizontal and vertical pulse-step generators are indicated by symbol size and colour, respectively.

Second, movement fields of cells for *small* saccades have a small diameter, when compared to cells associated with large saccades. It turns out that the diameter of the movement field increases roughly linearly with saccade amplitude (cf. with the retinal receptive field, above!).

Now, consider the following: since SC cells are not tuned to a delta-peaked function of saccade vectors, it must be concluded that whenever a saccade is made, say with amplitude R_o and direction Φ_o , a large *population* of cells in the SC will be recruited (namely all cells for which (R_o, Φ_o) belongs to the movement field). It may be expected, that the center of this population will correspond to the

coordinates prescribed by the neural mapping function, Eq. 53. An interesting further question is, what *shape* the population has in the SC motor map, and how it explains the properties of the movement fields.

4.3.2 Population coding of saccades in the SC motor map

The following hypothesis has been proposed to account for the shape and size-relation of the movement fields: when the skewed movement fields of many SC cells are replotted in SC coordinates (by applying the mapping function, Eq. 53) the following interesting property emerges:

- Each remapped movement field is *invariant* of the SC site. In other words, the size of the remapped movement field is roughly equal for all sites, and also the asymmetry disappears so that the remapped fields are rotation-symmetric (Fig. 43, bottom left).

Conceptually, the remapping of a movement field into SC coordinates leads to a reconstruction of the actual *population* activity profile in the motor map (provided the movement fields for cells at identical sites are also identical). Thus, the data indicated that the size and shape of the population of cells in the SC is identical for each saccade, only its *location* within the motor map changes for saccades of different amplitudes and directions (see Fig. 43, center panel left).

In summary, the population activity function in SC coordinates can be well described by a *rotation-symmetric, shift-invariant, gaussian* (Fig. 43, bottom left):

$$F(u, v) = F_o \cdot \exp \left(-\frac{(u - u_o)^2 + (v - v_o)^2}{2\sigma_o^2} \right) \quad (54)$$

with F_o , and σ_o *fixed* parameters (the same for every site in the SC, and $\mathbf{w}_o = (u_o, v_o)$ corresponds to the center of the population activity which is given by the afferent mapping function Eq. 53). Recordings from a large number of SC cells have indicated that an optimal choice of parameters for the population activity profile is: $F_o \approx 500$ Hz, and $\sigma_o \approx 0.5$ mm.

Connection scheme of SC with the brainstem: The next question then is, how such a population of activated SC neurons will have to project to the brainstem pulse-step generators in order to encode the correct, goal-directed saccade vector. In principle, there may be many ways in which the SC could encode the saccade vector, but the following simple model captures a biologically plausible way (because it is simple). According to this model, the following principles apply (see Fig. 43, center panel):

- [1] All cells that are recruited within the gaussian population contribute to the saccade (i.e. not only the center (few) cells!). The model therefore constitutes a *population coding scheme*, or '*coarse coding*' scheme.
- [2] Cells that have a high firing rate yield a larger contribution to the saccade vector than poorly active cells (like in a democracy!).
- [3] The resulting saccade vector is finally determined by a *weighted sum* of all cell contributions.

The synaptic weightings for each neuron of the population are determined by two factors:

- (1) each cell's firing rate (which varies from saccade to saccade), and
- (2) by each cell's synaptic connection strength with the brainstem (which is *fixed!*).

The latter property of the SC map is called the *efferent mapping function* (= output, or motor mapping) of the colliculus (see also Exercise 4.3) and depends exclusively on the *location* of each cell within the motor map (see Fig. 35, center right). Thus, to summarize,

$$\mathbf{z}_o = \sum_{i=1}^N F_i \cdot \mathbf{W}_i \quad (55)$$

with \mathbf{z}_o the saccadic movement vector, (the desired 2D displacement vector) $(\Delta x, \Delta y)$, F_i , is the firing rate of cell i in the active gaussian population ($F_i \in [0, F_o]$), and \mathbf{W}_i represents the efferent synaptic weighting of cell i with the horizontal and vertical pulse-step generators in the brainstem.

Conceptually, Eq. (55) entails that each cell in the population generates a small 'mini-vector' to the brainstem, the size of which is modulated by its firing rate. At the level of the brainstem all contributions are linearly summed, and this should exactly yield the required saccade vector. The question is, however, whether the gaussian weighting of the firing rates is adequate to fulfill this latter requirement. Although it is analytically very difficult to show that Eq. 55 indeed yields the correct saccade components to refixate the target, computer simulations have shown that this is indeed the case.

In the following chapter we describe a detailed neuro-computational model that explains how activity of SC cells contributes to the generation of the saccadic eye movement. We show how neurophysiological experiments have demonstrated that:

1. the population of SC cells encodes a straight eye-movement trajectory
2. the number of spikes in the SC burst determines the cumulative eye-movement displacement
3. the saccade velocity is determined by the height of the firing rate of the SC cells
4. the SC motor map encodes the nonlinear main sequence of saccades, i.e. brainstem burst cells can be linear.
5. the SC population acts as a *dynamic vectorial pulse generator* for saccades (Common Source).

4.4 Exercises

Problem 4.1:

In the ‘Common Source’ model of the saccadic system, the brainstem is driven by a nonlinear vectorial pulse generator that transforms a 2D motor error vector, Δe_{vec} , into a vectorial eye-velocity command according to:

$$\dot{e}_{\text{vec}}(t) = v_{\text{max}} \cdot [1 - \exp(-|\Delta e_{\text{vec}}(t)|/m_o)]$$

with $|\cdot|$ the magnitude of the vector.

Give expressions for the velocity profiles of oblique saccades $[R, \Phi]$, with identical horizontal saccade components (i.e. horizontal component amplitude is fixed, say at ΔH , but the vector rotates over angle Φ with respect to the horizontal direction).

Problem 4.2:

The complex-log map has a singularity at $\mathbf{z} = \mathbf{0}$. In order to provide a more realistic model for the neural mapping onto the visual cortex, the singularity has to disappear. Therefore, a simple extension of the map is given by the following function:

$$\mathbf{w} = \ln(\mathbf{z} + \mathbf{a})$$

where $\mathbf{z} \equiv (x, y)$, and $\mathbf{a} \equiv (1, 0)$.

Make a 2D graph of this new complex-log mapping function (as in Fig. 42). Give a mathematical prescription for the inverse mapping of this function: $\mathbf{z} = M^{-1}[\mathbf{w}]$.

Problem 4.3:

The complex-log mapping of the superior colliculus is given by Eq. 53.

Give an expression for the *inverse* mapping function (the *efferent map*) that relates the horizontal (Δx), and vertical (Δy) saccade components ($\mathbf{z}_o = (\Delta x, \Delta y)$) to the collicular neural coordinates, $\mathbf{w}_o = (u_o, v_o)$:

$$\mathbf{z}_o = \text{EFF.MAP}(\mathbf{w}_o)$$

Problem 4.4 (a bit more challenging):

Suppose that the brain somehow selects the center of the active gaussian collicular cell population and that the center determines the size and direction of the saccade vector, $\Delta \mathbf{e}$.

Assume that this selection process is noisy, so that the center of the population (in response to identical target presentations) varies from saccade to saccade. Suppose that the scatter is described by a small circular region within the collicular complex-log map.

Derive an expression for the distribution of saccade vector endpoints that results from this scatter, and show that under these assumptions the anisotropy of the motor map (the finding that $B_u \neq B_v$) is directly reflected in the saccade endpoint distribution.

5 The SC acts as a Vectorial Pulse Generator

5.1 The blink-perturbation paradigm in the SC

In the previous chapter we saw that neurons in the deeper layers of the SC discharge for saccades to a restricted region in the visual field (the cell's movement field), and form a topographic map of saccade amplitude, R , and direction, Φ . Electrical microstimulation of cells through an electrode in the SC elicits saccade vectors that closely match the movement fields of the stimulated cells. Earlier models of the SC have assumed that only the *location* of the active cell population determines the saccade vector, and that its temporal discharge patterns have no relation to the saccade trajectory and/or kinematics. The latter were thought to be controlled by a nonlinear feedback circuit in the brainstem (see Scudder's model, described earlier).

In recent years, however, accumulating evidence has suggested that the SC activity levels do influence saccade kinematics. For example, it was found that low firing rates in the SC are usually associated with slow saccades. Also, the intensity, number, and frequency of microstimulation pulses systematically affect both amplitude and velocity of saccades evoked at a particular SC site. Furthermore, the discharge of many SC cells has been reported to be related to the dynamic eye motor error, rather than to a static desired eye-displacement signal. All this evidence notwithstanding, controversy remains about the spatial-temporal transformation of SC activity patterns into appropriate commands for the horizontal and vertical brainstem saccade generators, largely because most studies have so far related SC activity to saccades with little variability and near-normal kinematics. In this section we briefly highlight experimental evidence, obtained from highly perturbed saccades and detailed spike-train analyses, to show that the dynamic activity patterns in the SC population carry all the information to encode the full saccade trajectory and kinematics. The evidence and ideas are described in more detail in the following studies:

- (1) HHLM Goossens and AJ van Opstal: Blink-perturbed saccades in monkey. I. Behavioral analysis. *Journal of Neurophysiology*, 83, 3411-3429, 2000
- (2) HHLM Goossens and AJ Van Opstal: Blink-perturbed saccades in monkey. II. Superior Colliculus activity. *Journal of Neurophysiology*, 83, 3430-3452, 2000
- (3) HHLM Goossens and AJ Van Opstal: Dynamic Ensemble Coding of Saccades in the Monkey Superior Colliculus. *Journal of Neurophysiology*, 95: 2326-2341, 2006 (found at: <http://www.mbfys.ru.nl/~johnvo/papers/scmodel.pdf>)
- (4) AJ Van Opstal and HHLM Goossens: Linear Ensemble Coding in Midbrain Superior Colliculus Specifies the Saccade Kinematics. *Biological Cybernetics*, 98: 561-577, 2008 (found at: <http://www.mbfys.ru.nl/~johnvo/papers/scmodel2008.pdf>)
- (5) RF Van der Willigen, HHLM Goossens and AJ Van Opstal: Linear visuomotor transformations in midbrain Superior Colliculus control saccadic eye movements. *The Journal of Integrative Neuroscience*, 10: 277-301, 2011
- (6) HHLM Goossens and AJ Van Opstal: Optimal control of saccades by spatial-temporal activity patterns in monkey Superior Colliculus. *PLoS Computational Biology* 8(5): e1002508, 2012 (found at: <http://www.mbfys.ru.nl/~johnvo/papers/PLoSCB2012.pdf>)

Recently, we studied SC activity during blink-perturbed saccades. Blinks change many aspects of behavior and SC responses that include eye velocity, saccade duration and spatial trajectories, as well as mean- and peak firing rate, and burst duration. Interestingly, both the *accuracy* of the saccades and the *number of spikes* in the SC burst remain unaffected (Fig. 36). Note that the actual 2D trajectories of the saccades are not reflected in the SC activity. The neuron in Fig. 36, for example, was not active for rightward saccades (i.e., saccade outside its movement field). Yet, when the eye moved rightward to compensate for perturbations of saccades into its movement field, activity persisted until the saccade ended.

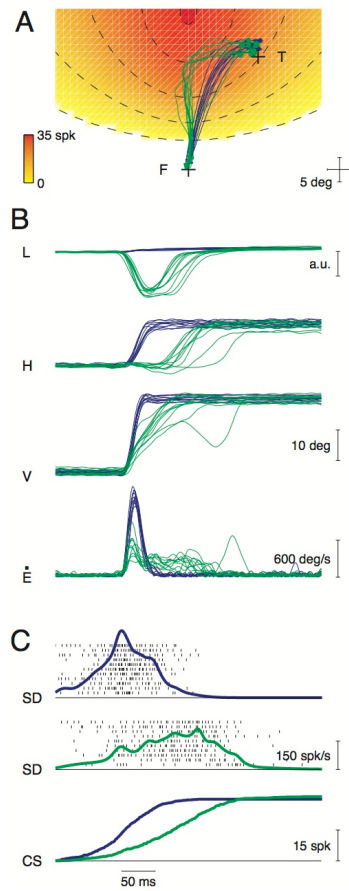


Figure 36. Activity of a SC neuron for control and blink-perturbed saccades.

Saccades were made from a fixation spot (*F*) toward a target (*T*) that was briefly flashed (50 ms) in the movement field of the neuron (color code). The 2D trajectories and traces of eye position ($H(t)$, horizontal; $V(t)$, vertical;) and track velocity ($\dot{E}(t)$) obtained in control trials (blue) illustrate the stereotyped nature of normal saccades. In perturbation trials (green), an air-puff-evoked blink

(eyelid traces, L) gave rise to strongly curved trajectories (A), a marked decrease in saccade velocity, and an increase in saccade duration (B). Mid-flight compensation ensured, however, that the eye reached its goal in darkness. Activity of the cell showed two major changes (C). The firing rate ($SD(t)$, spike density) reduced considerably, and the burst duration increased, roughly matching the increase in saccade duration. Even so, the total number of spikes in the burst was unaltered as indicated by the cumulative number of spikes ($CS(t)$).

Based on these findings we here propose and test the hypothesis that each spike from a SC neuron adds a site-specific, infinitesimal displacement vector to the dynamic SC movement command. According to this proposal, the cumulative number of spikes of each cell correlates with the amplitude of the instantaneous eye displacement component in the direction of the intended saccade vector.

5.2 Spike-train analysis of SC saccade bursts: dynamic movement fields

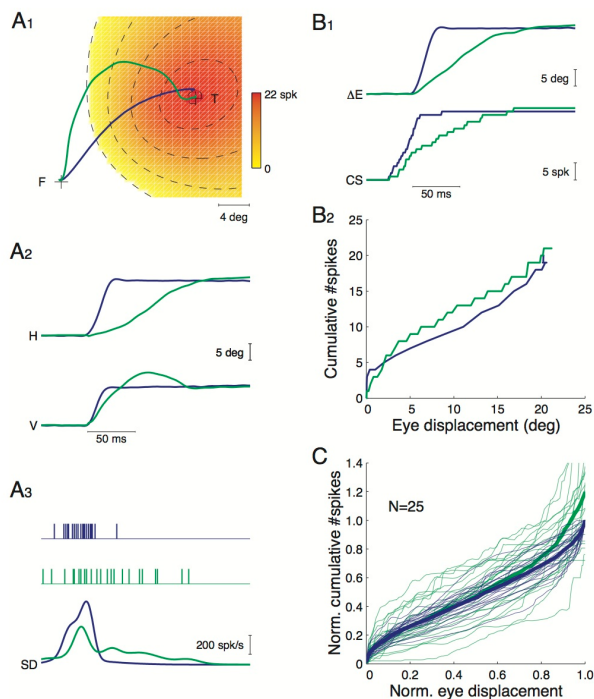


Figure 37. Cumulative number of spikes reflects instantaneous eye displacement.

(A): Raw data from a representative control (blue) and perturbation trial (green). (B): Eye displacement, $\Delta E(t)$, was calculated along the straight line connecting starting and end point of the saccade. The cumulative number of spikes, $CS(t)$, was determined by counting spikes from 20 ms before saccade onset (B_1). The spike-count data were delayed to roughly align saccade and burst onsets ($\Delta t = 20$ ms), and the dynamic relation between $CS(t)$ and $\Delta E(t)$ was examined by plotting one variable against the other (B_2). Note that two experimental conditions yield very similar, roughly linear response curves. (C): Normalized response curves for control (blue) and perturbed

green) saccades toward the movement field center for all 25 SC neurons tested in this way. The average population response is virtually identical for the two experimental conditions (thick curves).

Figs. 37A-B illustrate our analysis for a typical SC cell, when the monkey made a saccade toward the center of its movement field during a control trial (blue) and a perturbation trial (green). From the raw data (Fig. 37A), we calculated the instantaneous eye displacement ($\Delta E(t)$; Fig. 37B₁) along the straight saccade trajectory (F-T) by projecting the actual eye position coordinates (H and V) onto the straight line connecting the initial fixation point and final end point. The cumulative number of spikes ($CS(t)$; Fig. 37B₁) was determined from 20 ms before saccade onset. Spike-count data were delayed by 20 ms and plotted as function of instantaneous eye displacement (Fig. 37B₂). This delay is based on the observation that the lead time of the saccade-related burst of SC cells relative to movement onset, as well as the latency of electrically evoked saccades, are in this range. Note that the resulting response curves for both the control and perturbed saccade follow very similar, roughly linear trajectories (Fig. 37B₂). Clearly, this is not just a consequence of a similar number of spikes in the burst; had the burst dynamics not been altered in the perturbed condition, the number of spikes would have been the same, but the response curve would have been totally different.

Fig. 37C shows that comparable results were obtained for all 25 neurons that could be fully tested in this way. Note that the population average of the perturbed responses (thick green curve) closely matches the average control curve (thick blue curve). Thus, it appears that for a given cell the cumulative number of spikes in the burst, delayed by about 20 ms relative to saccade onset, provides a good descriptor of the instantaneous displacement of the eye along its desired straight trajectory, regardless the actual 2D trajectory.

For each neuron, we further quantified these relations for responses in different parts of the movement field using linear regression. Fig. 38A exemplifies this analysis for a typical SC neuron, when the monkey made saccades to five different targets (1-5). Note that there is a tight, near-linear relation in all five cases and that the control (blue) and perturbed (green) data yield very similar regression lines (solid). Moreover, there is an almost fixed final number of spikes in the burst, which differs systematically for each saccade vector according to the cell's movement field properties. For example, the burst for control and perturbed saccades toward the center of the movement field (Fig. 38A₁) contained ~ 25 spikes whereas this number dropped to ~ 10 spikes for the control and perturbed saccades in Fig. 38A₂. This difference across saccade vectors is reflected also in the *slopes* of the regression lines. For example, the slopes of the two regression lines in Fig. 38A₁ are much steeper than the ones in Figs. 38A₂ because the movement vectors in the former are closer to the neuron's optimum.

Figs. 38B-C summarize the regression results for all 25 neurons tested in this way. Filled symbols (●) denote responses toward the center of the movement field. Open symbols (○) correspond to off-center responses. For the far majority of cells, the slopes of the regression lines are about the same for the control and perturbed conditions (Fig. 38B), despite considerable differences in kinematics and 2D trajectories of the saccades. In addition, there appears to be a strong correlation between the cumulative number of spikes and the instantaneous eye displacement for both optimal and non-optimal saccade

vectors, as well as for both experimental conditions (Fig. 38C).

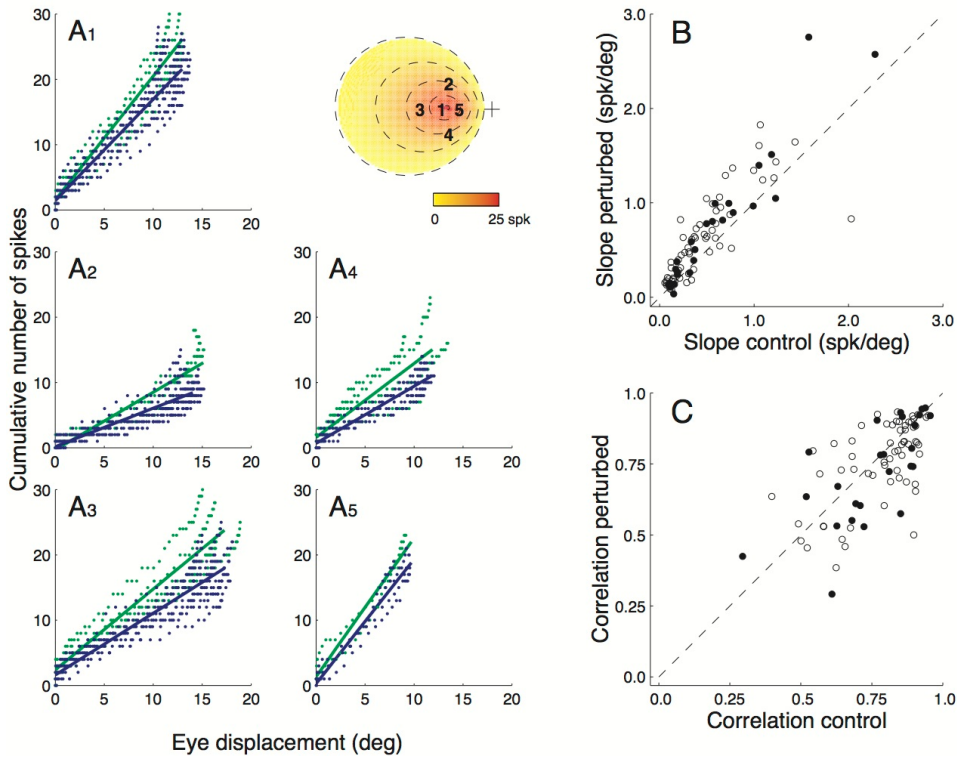


Figure 38. Dynamic movement field description.

A: Cumulative spike-count versus eye-displacement curves of control (blue) and perturbed (green) responses of a typical SC neuron for saccades to five different locations (1-5) in its movement field. Control and perturbation data are largely overlapping, and regression lines (solid) fit the data quite well under both experimental conditions. The total number of spikes in the burst as well as the slope of the regression lines varies systematically according to the cell's movement field. B-C: Regression results for all 25 SC cells tested in the blink-perturbation paradigm. Filled (●) and open symbols (○) denote results for saccades to the center and to more peripheral movement field locations, respectively. Dashed lines are identity lines. Note that the slopes (α) of the regression lines are very similar between the control and perturbed condition (B) and that the correlation values (r) are high under both conditions (C).

Figs. 37 and 38 indicate that each spike in the burst is associated with a small incremental displacement of the eye along the intended, straight trajectory. Obviously, the discharge of an individual SC neuron cannot really encode the desired eye displacement since there is no unique relationship between the cumulative number of spikes and the instantaneous eye displacement for different movement vectors (Fig. 38A). Interestingly, however, it appears that this dynamic relationship depends systematically on the saccade vector within a cell's movement field. In fact, our dynamic vector summation hypothesis implies that the relation between the cumulative number of spikes in the burst of a particular cell and

the instantaneous eye displacement during any saccade into its movement field of can be predicted from:

$$CS(t + \Delta t) = \frac{N_b(R, \Phi)}{R} \cdot \Delta E(t) \equiv \alpha(R, \Phi) \cdot \Delta E(t) \quad (56)$$

where $N_b(R, \Phi)$ is the cell's static movement field description that specifies the number of spikes in the burst as function of saccade amplitude and direction as described in the previous chapter. Δt is a fixed 20 ms delay between neural data and the ensuing eye movement, and $\alpha(R, \Phi)$ is the slope of the dynamic movement field relation.

Because quantitative predictions of SC discharge dynamics have not been tested so far, we first analysed the activity patterns of 73 neurons, recorded throughout the SC motor map, for normal visually guided saccades. As illustrated in Fig. 39A for a typical cell, the static movement field fits ($N_b(R, \Phi)$) were used to predict the cumulative number of spikes in the burst as function of the instantaneous eye displacement (at 2 ms resolution), as well as the slope of this relation for individual responses (Eqn. 56).

Data were obtained for many saccades scattered throughout a cell's movement field (typically, $n > 100$ for each cell), but for clarity Fig. 38A₁ only shows the results for a cross section in amplitude (*green*) and direction (*blue*). Note that the cumulative number of spikes is predicted quite well for all individual saccades (Fig. 38A₁), despite considerable variation in saccade metrics, kinematics and total numbers of spikes in the bursts. Accordingly, the predicted slopes were closely in line with those of the measured response curves for all saccades into the cell's movement field (Fig. 38A₂; $n = 319$). Fig. 38B shows that high correlations between the measured and predicted discharge patterns were obtained for the entire population of 73 SC neurons (population average, $r = 0.83$), indicating that the dynamic movement field model of Eqn. 56 provides a good description of the neurons' temporal discharge patterns. This is quite remarkable given that the model has only four free parameters (i.e., optimal saccade amplitude and direction, total number of spikes for the optimal displacement vector, and spatial tuning width), none of them having an explicit relation to the discharge dynamics.

Figs. 39C-D demonstrate that very similar results were obtained for the blink-perturbation paradigm. For these cells, the static movement fields were estimated from independent data sets of normal saccades ('movement field scans'). Still, the number of spikes in the burst (Fig. 39C₁) as well as the slopes $\alpha(R, \Phi)$ of Eqn. 56 (Fig. 39C₂) were predicted quite accurately for all control responses (*blue*). Even for blink-perturbed responses, the predicted slopes corresponded closely to the actual data (*green*, Fig. 39C₂). Only the number of spikes in the burst was typically underestimated (Fig. 39C₁, Discussion). Fig. 39D quantifies the overall correlation between the measured and predicted cumulative number of spikes. For the far majority of cells, the correlation appears to be comparable for both experimental conditions, despite considerable differences in kinematics and 2D trajectories of the saccades.

To test the hypothesis that linear vector summation of the movement tendencies provided by each spike in the SC population can be used to decode the dynamic eye movement command, we applied the raw data from all 73 SC neurons to a linearized 2D version of Scudder's (1988) model (Fig. 40A; see also previous section, for details).

Briefly, the location of each neuron in the SC motor map was determined from the center of its movement field. For each point in time, we then estimated the instantaneous SC population activity from the

measured spike events at each recording site by calculating spatially smoothed maps of the instantaneous firing rates, starting 20 ms before saccade onset.

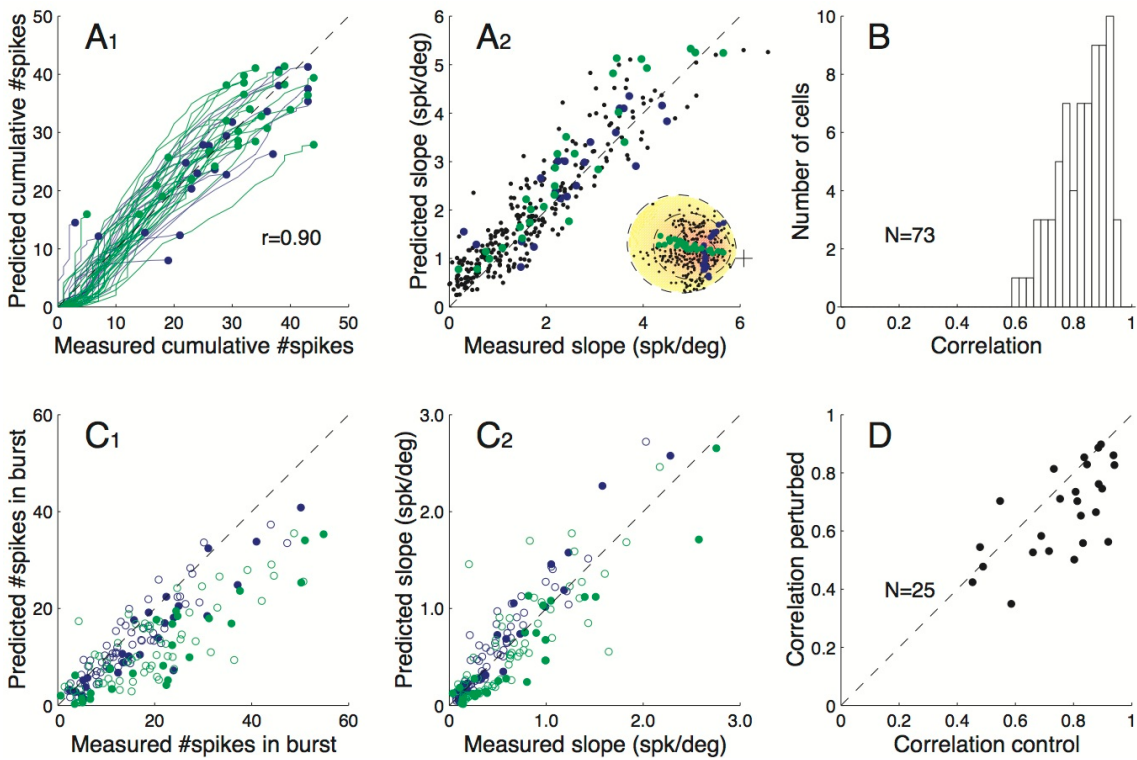


Figure 39. Prediction of SC discharge dynamics

A: Predicted vs. measured cumulative spike count during normal saccades of different amplitudes (green; $n=21$) and directions (green; $n=28$) into the movement field of a SC cell (inset A₂). All curves run closely to the identity line (dashed; $r=0.90$). Accordingly, the slopes of the response curves were predicted quite accurately (A₂; $n=319$). B: High correlations between data and model (Eqn. 56) were obtained for all SC neurons tested with visually guided saccades into the movement field. C: For the 25 SC cells in the blink-perturbation paradigm, the spike count (C₁) is slightly underestimated in the perturbed condition, but the slopes of the response curves are predicted remarkably well under both conditions (C₂). Responses towards the center (●) and more peripheral (○) movement field locations (c.f., Fig. 37A) are indicated separately. D: The correlation between data and model was hardly affected by the blink-evoked disturbances, for practically all 25 SC cells in which appreciable blink-perturbations were obtained.

The brainstem circuitry for the horizontal and vertical eye-movement components was modeled by two independent *linear* feedback systems. Only four parameters had to be optimized: two scaling factors, γ_x and γ_y (identical for all cells), that scaled the site-specific horizontal (m_x) and vertical (m_y) SC projection strengths to the brainstem, the feedforward gain, B , of the brainstem pulse generators, and a fixed delay in the feedback loops.

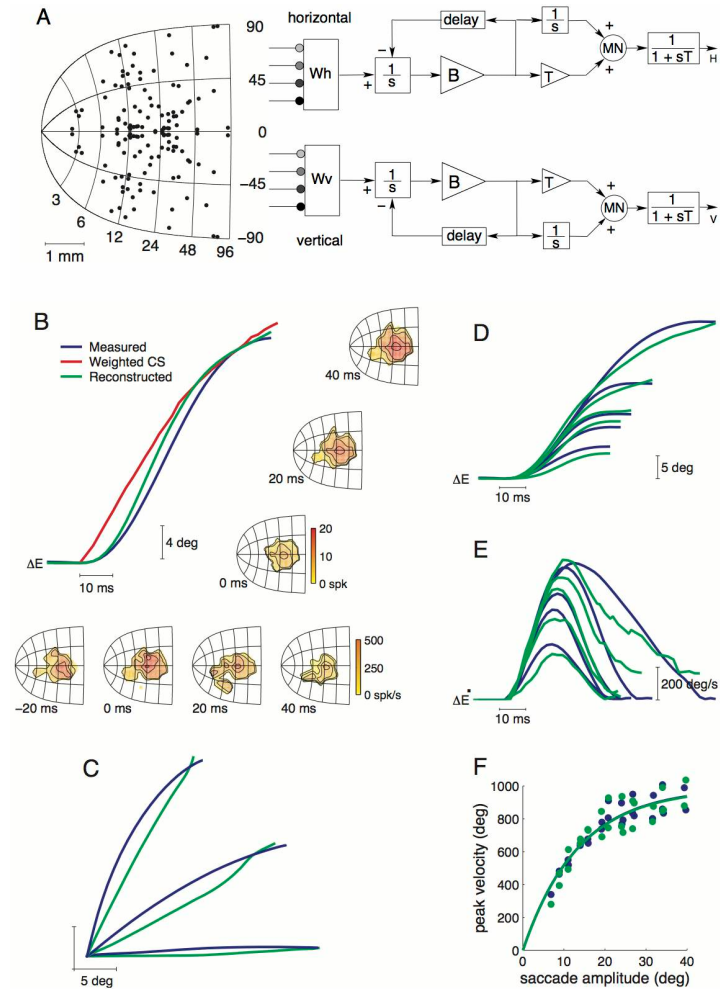


Figure 40. Saccade reconstruction from recording SC spike trains of 139 cells.

A: Linear 2D model of the SC-brainstem saccade generator. Recording sites are indicated in the SC motor map. m_x , m_y , SC projection strengths to the brainstem with scaling factors $\gamma_x = 4.0 \cdot 10^{-3}$ and $\gamma_y = 2.7 \cdot 10^{-3}$, respectively; $B = 100$ spk/s/deg, forward gain of the burst generators; Delay = 7 ms, delay in the feedback loop; $T = 150$ ms, time constant of eye plant. B: Profiles of a measured (blue) and reconstructed (green) horizontal saccade with maps of the instantaneous firing rate, $f_i(t)$ (bottom). Maps of the cumulative spike count at each site (right) were obtained by temporal integration of the instantaneous firing rates. C: Although the model assumes independent horizontal and vertical brainstem burst generators, 2-D trajectories of reconstructed saccades in different directions were virtually straight. D-E: Reconstructions produced realistic eye displacement ($\Delta E(t)$) and eye velocity ($\Delta \dot{E}(t)$) profiles for saccades of different amplitude ($R = [7, 11, 14, 21, 35]$ deg). F: The non-linear amplitude peak velocity relationship of normal saccades appears to be embedded in the SC activity patterns.

Fig. 40B shows the reconstruction result for a horizontal saccade, together with the corresponding population activity in the SC motor map at different moments in time relative to saccade onset. Note that the activity stays at the same motor map location during saccade execution. Furthermore, the

reconstruction (*green*) generated a realistic saccade profile that closely matched the (average) measured saccade (*blue*). Fig. 40C illustrates that the reconstructions yielded approximately straight trajectories, not only for horizontal saccades but also for oblique saccades. One should realize, however, that this property is entirely due to the spatial-temporal distribution of activity in the SC motor map. Figs. 40D-E show that also the position traces and velocity profiles of saccades with different amplitudes are predicted quite well by the model. For example, the reconstructions reproduced both the bell-shaped velocity profiles of small saccades and the skewed velocity profiles of large saccades. Fig. 40F shows that the amplitude - peak velocity relation ("main sequence") for reconstructed saccades (*green*) equals that of the measured (*blue*) saccades. Note, however, the brainstem circuit in the model is entirely linear. Hence, the dynamic non-linearity in the saccadic system underlying the main sequence relations appears to be entirely embedded in the SC activity patterns.

5.3 The nonlinear vectorial pulse generator concept.

According to the dynamic population-coding model of Fig. 40, the instantaneous firing rates of cells in the active SC population influence the desired velocity of the eye along its intended (straight) eye-movement trajectory. Computer simulations with the model suggest that (1) straight saccade trajectories, and (2) the nonlinear main sequence characteristics of saccade kinematics are entirely due to the spatial-temporal distribution of activity within the SC. The motor SC could thus be considered to embody a vectorial nonlinear pulse generator. The brainstem pulse generators decompose this dynamic vectorial signal into appropriate commands for the eye muscles (see the description of the "Common Source model" in the previous part of this Lecture).

Our results indicate that the SC represents straight saccade trajectories and kinematics in the direction of the desired eye-displacement vector, but not that such is determined by efferent feedback at the level of the SC. SC cells appear to be unaware of the blink-induced curvature of the eye movement and of the subsequent compensatory phase (Fig. 40), suggesting they do not receive feedback about the actual 2D trajectory of the eye. Rather, we propose that compensation for the perturbations is due to an error-corrective mechanism that acts downstream from the SC (Fig. 40).

5.4 Part 3: Computer simulations with saccade-lin.mdl: a nonlinear SC pulse generator

Now that we have seen that the Brainstem Burst generator can be modeled as an entirely *linear* feedback system, and that the SC neural population may act as a nonlinear pulse generator, we will play a bit with the Scudder saccade model to implement this idea. To that end, the nonlinear burst characteristic of the Scudder model has now been replaced by a simple linear gain (value $B=80$), and the invariant burst in the SC of that model is now a burst that varies its properties (duration and pulse height) as function of the saccade amplitude.

Load the model **saccade-lin.mdl** and run it in its default settings to verify that indeed it produces normal saccades. In what follows, we will generate two sets of computer simulations with this model

for saccade amplitudes of $R = [2, 5, 10, 15, 20, 30, 40, 50]$ deg. The different amplitudes are obtained by varying the synaptic gain of the SC output (this symbolizes the different projection strengths from the SC motor map to the brainstem burst generator).

Set 1 Generate the saccades and measure (like in the previous model simulations) on the oscilloscope of the saccade velocity profile the saccade duration and peak velocity. Plot the main sequence of the saccades. What do you see?

Set 2 We will now generate the same set of saccades, but for each saccade we toggle a bit with the SC burst properties. To that end, apply the following recipe:

- (a) Burst duration increases with saccade amplitude according to $D_{\text{burst}} = a \cdot R_{\text{sacc}} + b$ with $a = 1.5 \text{ ms/deg}$ and $b = 20 \text{ ms}$.
- (b) Whatever you do to the SC burst, the number of spikes should remain constant!

Generate the saccades and measure the main sequence. Also plot the associated SC bursts. Conclusion?

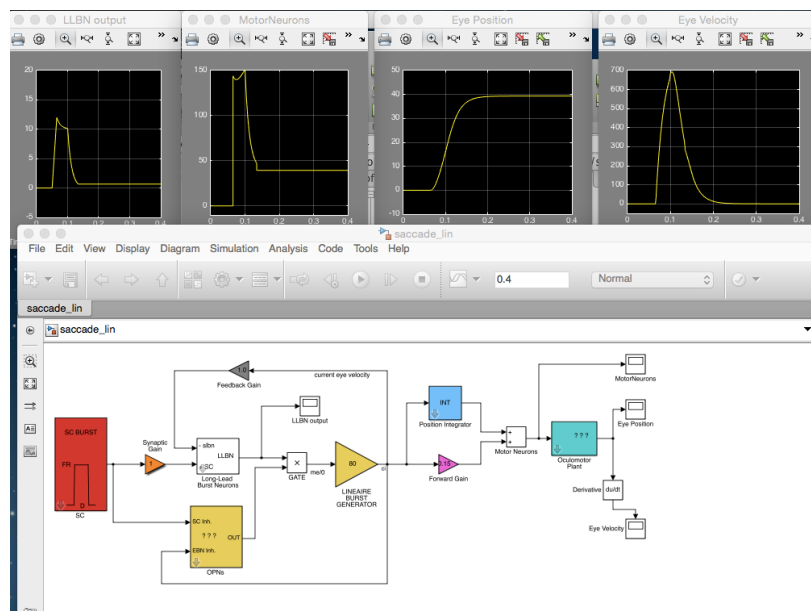


Fig. 41 Default output of model *saccade-lin.mdl*

6 Extra Material: Intro Eye-Head Coordination

Here, I will highlight some of the different approaches to the more challenging problem of how the brain might coordinate the eyes and head in fast, saccadic gaze shifts (n.b.: gaze = the orientation (commonly called: the 'position') of the eye (read: fovea) in space). This material will not be covered in my lectures on June 30, but may serve as an overall introduction to eye-head coordination into which dr. Stefan Glasauer will go into much more depth on July 2.

Students may want to glance through the following paper for the background and exercises (pdf available at <http://www.mbfys.ru.nl/~johnvo/papers/eyehead.pdf>):

HHLM Goossens and AJ van Opstal: Human eye-head coordination in two dimensions under different sensorimotor conditions. *Experimental Brain Research* **114**: 542-560, 1997

With the body fixed in space, but the head free to rotate on the neck, the gaze direction in space is approximated by¹:

$$G_S = H_S + E_H \quad (52)$$

with H_S the head orientation on the neck/body (space), and E_H the eye orientation in the head. A *gaze shift* (or gaze saccade) is the change in gaze direction, and is here denoted by ΔG . Yesterday, we dealt with head-fixed eye movements (the saccadic system, and the VOR during whole-body rotation). Note that all eye-movement excursions are constrained by the so-called oculomotor range, which for cats is only about 25 deg around the straight-head direction, and for monkeys and humans up to about 35-40 deg. The largest head-restrained primate saccadic eye movement is about 80 deg, when made from the far left fixation point (at -40 deg) to the far-right fixation point (at +40 deg). Clearly, orienting eye-head gaze shifts can be made over a much larger range, and even when the eyes and head are initially fixating at straight ahead, a gaze shift of about 100 to 120 deg (in barn owls even over 180 deg!) can be readily generated.

6.1 A problem for gaze control

In the lecture of prof Galiana we have seen that the function of the VOR is to keep the eyes stable in space by counteracting head movements. This stabilizing reflex is useful (and mandatory) when foveating a particular target while moving through space. However, in an eye-head gaze shift steady fixation needs to be broken, in which case the operation of the VOR may not be beneficial:

During saccadic gaze shifts eyes and head should move in the *same* direction; however, the slow-phase VOR makes eyes and head move in exactly *opposing* directions.

¹In 1D Eqn. 41 is exact; in 2D it's a reasonable approximation within the frontal movement space, but in 3D, non-commutative rotational algebra should be used to describe the gaze direction. This topic is beyond the scope of this course.

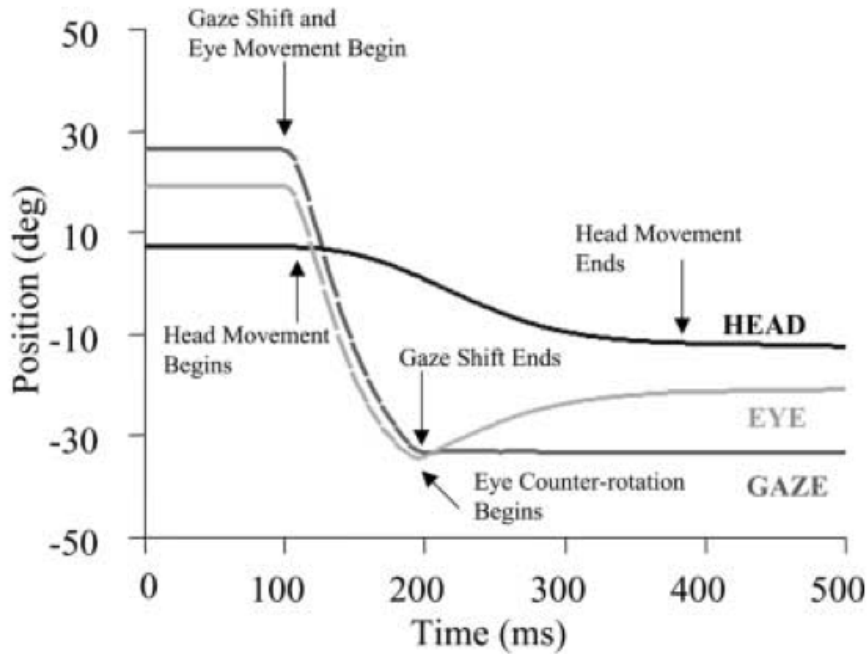


Fig. 42 Gaze, eye- and head displacements as function of time for a leftward horizontal gaze shift. Note that at gaze offset the eye starts to counterrotate in the head. In this example, the eyes started from 15 deg to the right.

Several researchers have therefore proposed that the VOR would be switched off at the start of the gaze shift, to enable the rapid change of gaze in the same direction as the head movement. However, since the head-movement kinematics are much slower than those of the eye during saccades, the eye-in-head would reach the limits of the OMR very rapidly, while the head would still move for several tens (even hundreds) of milliseconds. With the VOR off, the eye-in-space would thus be carried by the head, but as soon as the fovea would reach the goal, the eye-in-space movement should stop, even though the head still continues to move. This would only be possible if the VOR would immediately turn on as soon as the eye is on target, so that the ongoing head movement would rotate the eye back towards the center of the OMR as a result of the VOR slow-phase. Figure 42 illustrates the temporal sequence of an eye-head gaze shift.

6.2 Reference frames

In the previous chapter we didn't touch the issue of reference frames, but here it may be useful to introduce this topic, especially since eye-head coordination involves different sensory and motor effectors (the visual stimulus on the retina, a sound entering the ears, the head rotating on the neck, the eye rotating in the head, the vestibular organ fixed in the head). Rather than reiterating the literature on this topic, we here illustrate the problem by examples.

6.2.1 Eye: driven by eye coordinates or head coordinates?

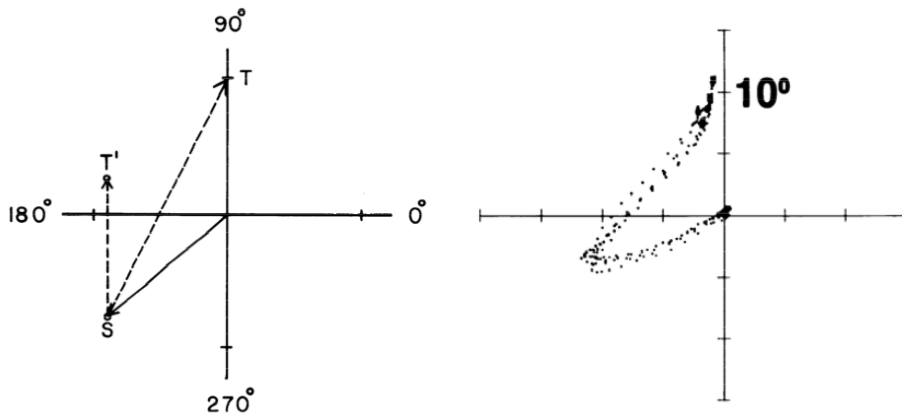


Fig. 43 Test for compensation of a perturbation in the programming of saccades: microstimulation in the SC (from Sparks and Mays, 1983).

It is generally thought that the pprf cells (horizontal eye-burst generator) encode an eye-velocity signal, and that the pprf cells themselves are driven by an eye-motorerror signal. It has been long recognized that the retinal signal alone is insufficient to explain saccade accuracy, if only for the simplest of situations (saccade to a single visual target in otherwise darkness). Double-step target experiments in darkness indicate that the eyes accurately incorporate intervening changes in eye position, so that some form of feedback is used by the saccadic system to update retinal target locations into a correct oculocentric motor command (note: this is *not* the local feedback loop that controls the saccade kinematics, like in Fig. 27! Let's call this target updating pathway a *global feedback loop*).

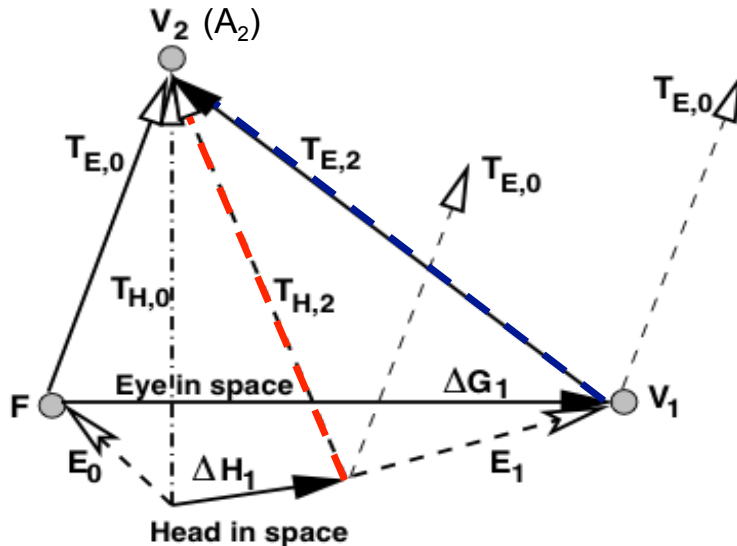
Figure 43 shows the result of a famous experiment by Sparks and Mays (*JNP*, 1983), in which the saccadic system programmed a correct response to a briefly flashed visual stimulus, even when the eyes were driven to a new position (in darkness) by microstimulation of the midbrain superior colliculus. This seminal experiment thus demonstrated that target updating even takes place in the absence of a motor plan! Moreover, the coordinates for the goal-directed saccade are represented by the SC cells. However, how the transformation is carried out by the brain has given rise to quite some controversy among researchers. For the head-fixed situation, two proposals have dominated the literature to explain saccades in response to a sequence of visual targets:

1. The eye motor error is derived by a two-stage transformation (Robinson's model; Andersen and colleagues): In the first stage the retinal target is represented in a 'suprarectal' reference frame (head-centered, body-centered, world-centered):

$$T_{\text{Head}}(t = 0) = T_{\text{eye}}(t = 0) + e_{\text{head}}(t = 0)$$
In the second stage, the head-centered target is transformed into a dynamic eye-centered motor error: $M_{\text{eye}}(t) = T_{\text{Head}}(t = 0) - e_{\text{head}}(t)$
2. The eye motor error is directly derived from the retinal input and from efference copies of eye-displacement (the Jürgens model; Goldberg and colleagues, Scudder): $M_{\text{eye}}(t) = T_{\text{Eye}}(t = 0) - \Delta e(t)$

The first scheme operates in absolute *position* coordinates, while the alternative model is expressed in relative *displacement* coordinates.

6.2.2 Coordinate transformations in eye-head gaze shifts



	2 nd eye movement:	2 nd head movement:
V ₁ V ₂	$T_{E,2} = T_{E,0} - \Delta G_1$	$T_{H,2} = T_{E,0} - \Delta G_1 + E_1$
V ₁ A ₂	$T_{E,2} = T_{H,0} - \Delta H_1 - E_1$	$T_{H,2} = T_{H,0} - \Delta H_1$

Fig. 44 Coordinate transformation problem for a double-step gaze shift, planned to a sequence of Visual-Visual or Visual-Auditory targets).

The coordinate transformation problem for combined eye-head gaze shifts in a double-step situation is considerably more complex than for the head-fixed condition, as is illustrated in the vectorial scheme of Fig. 44. Here, at the start of the gaze shift, the eyes and head are not aligned in space (the eye looks at F , but its orientation is left-upward in the head), and a first gaze shift is planned to a visual flash at V_1 . Note that the eye-movement and head-movement have different trajectories toward V_1 , which means that after the gaze shift the coordinates of the second target are quite different for eyes ($T_{E,2}$) and head ($T_{H,2}$). The dotted arrows ($T_{E,0}$) indicate the hypothetical trajectories if both would be driven by the initial (retinal) target coordinates. The equations show the required vector transformations for the eyes (blue arrow) and head (red arrow) when the second target is a visual flash (first row), or an auditory noise burst (second row). Behavioral experiments have shown that the gaze-control system follows the predictions given by these equations, even when the second target was presented in midflight of the first gaze shift! (Vliegen et al., 2004).

6.2.3 Eye-head gaze shifts: behavioral data

Two-dimensional eye-head gaze shifts to visual and auditory targets with unaligned initial conditions have demonstrated that the eyes and head are indeed goal-directed, as required by the transformations in Fig. 44. In Fig. 45 the different reference frames (eye-, head-, and body-centered coordinates for a target) are highlighted, in conjunction with the oculomotor range that restrict the movements of the eyes.

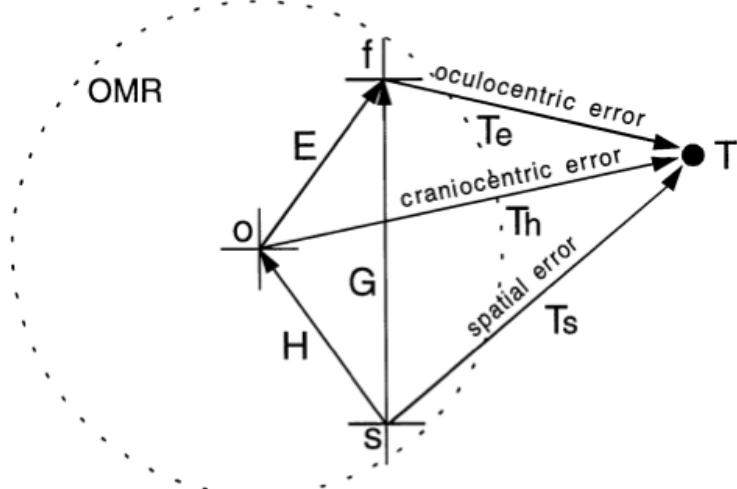


Fig. 45 Reference frames for a target in space. OMR: oculomotor range around the o (the center of the head); f the fovea; s the origin of the head rotation point. H the head-on-body orientation; E the eye-in-head orientation; G the gaze orientation (Eqn. 41). T_e the target location relative to the eye (retinal error, or initial gaze error); T_h the head-motorerror and T_s the error in world coordinates.

Several questions arise that have been addressed by at least as many different models of the gaze control system:

- How does the gaze-control system switch between the different behaviors of the VOR?
- What is (are) the driving signal(s) for the eyes and head?
- How does the system monitor whether or not the eyes have reached the goal?
- Is the gaze-control (i.e. eyes and head) system driven by internal feedback? What type of feedback signal(s)?
- Do eyes and head indeed move in the same directions?
- Are eyes and head movements initiated simultaneously?
- What is the signal carried by the saccadic burst generator?
-

Figure 46 shows the results of a visual and auditory localization experiment with unaligned initial eye- and head orientations (data from Goossens and Van Opstal, *EBR*, 1997). Clearly, (i) the movement

directions of the eyes and head are towards the goal, and (ii) they are the same for the visual and the auditory target, despite the different underlying coordinate transformations (see Fig. 44).

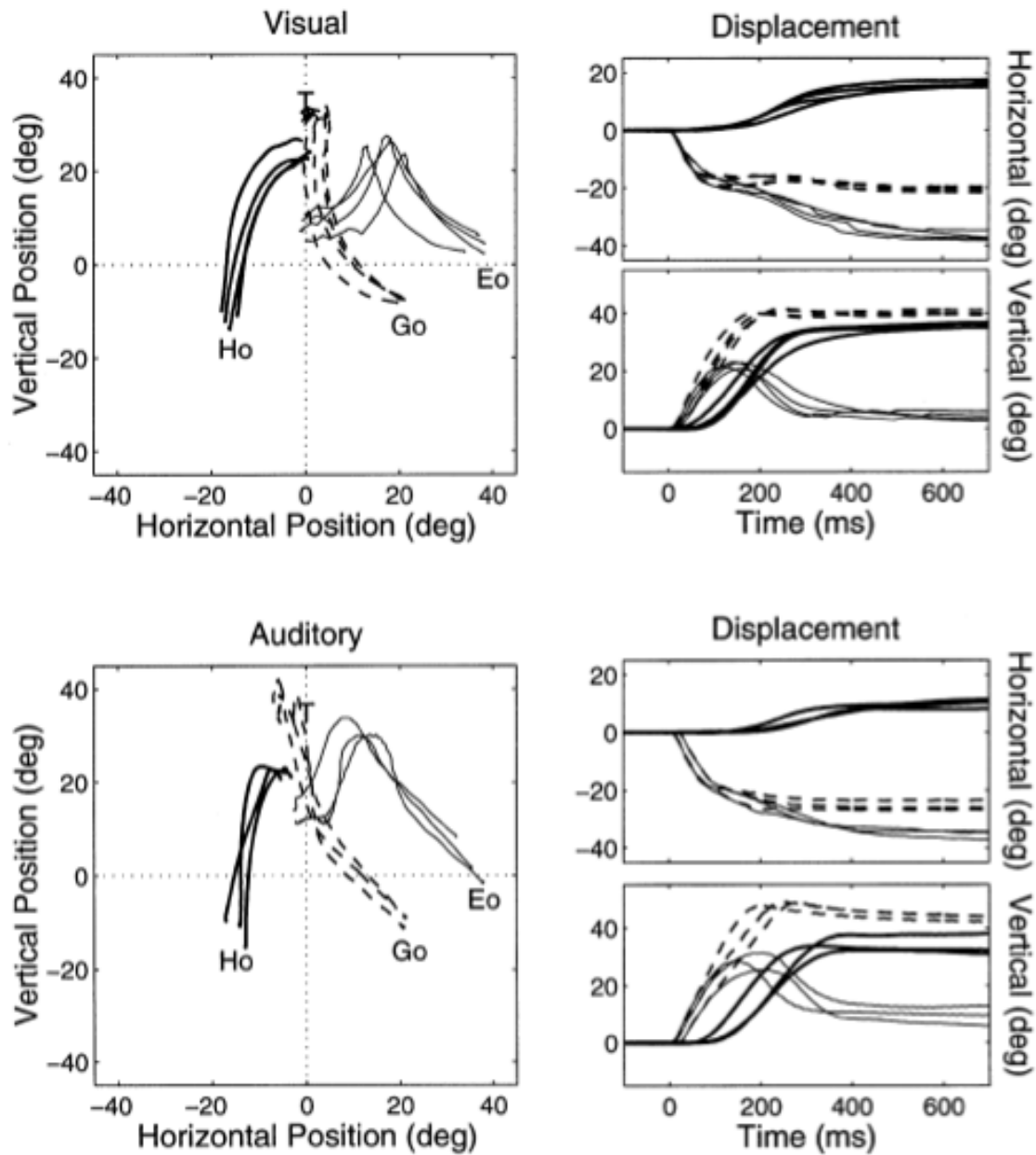


Fig. 46 Measured gaze-, eye-, and head-movement trajectories in space or visual- and auditory-evoked gaze shifts (eye movement is plotted in head-centered coordinates). Eyes and head move in the direction of the target.

6.3 Gaze-control models

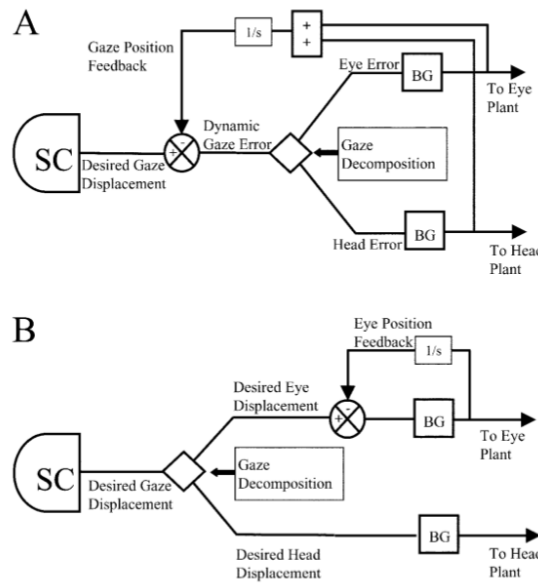


Fig. 47 Two alternative gaze-control models, both driven by a collicular ΔG signal. (A) Gaze motor error is decomposed into separate eye- and head-motor error signals that drive separate (interacting) burst generators (BG). The scheme utilizes gaze feedback. (B) The decomposition of ΔG is upstream from the eye- and head controllers, and only the eye is driven by local feedback.

Figure 47 (from Freedman, *Biol. Cybernet*, 2001) shows two fundamentally different proposals as to how eye-head gaze shifts could be programmed by the central nervous system. The fundamental difference here is whether the system is under gaze-feedback control (scheme in Fig. 47A) or not (scheme in Fig. 47B). Both models predict essentially identical gaze-shift trajectories, even under intervening head-movement perturbations, and as such cannot be readily dissociated on the basis of a behavioral experimental protocol². In what follows, relevant for the computer exercises this afternoon, we will focus on two control schemes forwarded over the years by the tutors, which both utilize gaze feedback (as in Fig. 47A):

1. An adapted version of a gaze-feedback scheme that puts the collicular gaze-displacement command *outside* the local gaze-feedback loop (after Goossens and Van Opstal (*EBR*, 1997)).
2. A gaze-feedback model in which the feedback signal *incorporates* the superior colliculus (after Galiana and Guitton, *Ann. NY Acad. Sci.*, 1992, and Prsa and Galiana, *JNP*, 2007).

²The models *do* predict different behaviors, however, for intervening perturbations of the *eye* movements, e.g. by an evoked blink. The scheme in B then predicts a localization error (no compensation), whereas the scheme in A predicts accurate gaze shifts. Goossens and Van Opstal (in preparation) obtained experimental support for the latter.

6.3.1 The PPRF output: eye- or gaze velocity?

In head-fixed saccades the saccadic burst of the pprf cells encode the instantaneous velocity of the eye in the head: $\dot{e}(t)$, and this signal is used to generate the 'hold' signal (eye position) for the oculomotor plant. But what about head-free gaze shifts? Studies (e.g. from Kathy Cullen and Dan Guitton) have suggested that the pprf burst carries information about both eye-in-head velocity, and head-on-neck velocity. This would suggest that these cells might transmit a gaze-velocity signal. Similar suggestions have been made by others (e.g. Ling et al., *JNP*, 1999) for recorded activity (number of spikes in the burst) of extraocular motoneurons (abducens). Especially this latter finding seems particularly strange, as these neurons directly innervate the eye muscle, and would therefore be expected to exclusively encode an eye-position/velocity-related signal, irrespective of the head movement. However, Cullen and Galiana (Cullen et al. *JNP*, 2000) demonstrated that the abducens spike-count analysis was based on a fallacy, and that the instantaneous firing rate of these cells indeed reflected the eye-kinematics only. But what about the premotor burst cells in the pons? Here, the situation may be a little bit more diffuse.

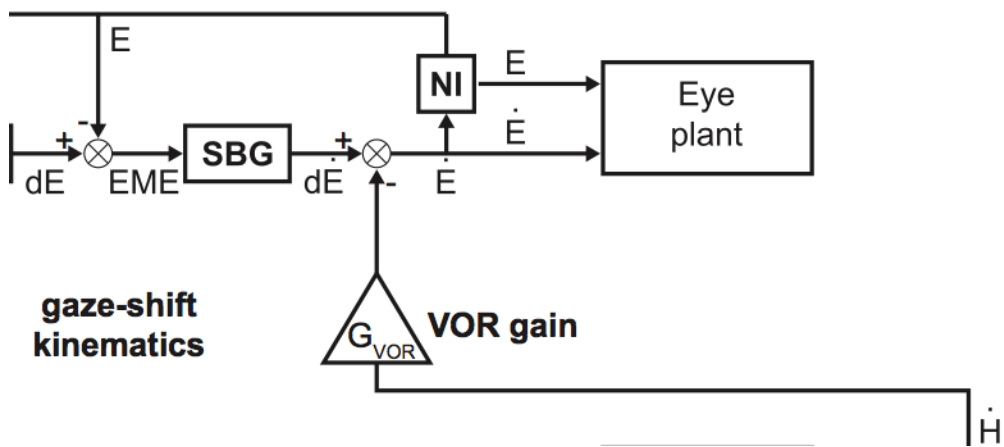


Fig. 48 In the Goossens and Van Opstal (1997) model, the output of the saccadic burst generator in the PPRF (desired eye velocity) is modified by the VOR. The oculomotor plant is driven by an eye-in-head velocity signal (as in Cullen et al., 2000).

Figure 48 shows a model interpretation of the PPRF - Abducence pathway, where the pprf activity is modified by the output of the vestibular system, but before the pulse-step generation stage. Let's denote the output of the pprf as a *desired eye-velocity* signal, \dot{e}_{des} . Suppose that the gain of the slow-phase VOR during a gaze shift is G_{VOR} , and could take any value between 0 (VOR off) and 1 (VOR fully on). The signal from the vestibular nucleus would then reflect $\dot{e}_{VOR} = -g_{VOR} \cdot \dot{h}$. Thus, the velocity signal sent to the abducens oculomotor neurons (the actual eye-movement signal) is:

$$\dot{e}_{head} = \dot{e}_{des} - g_{VOR} \cdot \dot{h} \quad (53)$$

from which it follows that:

$$\dot{e}_{des} = \dot{e}_{head} + g_{VOR} \cdot \dot{h} = g_{VOR} \cdot \dot{g} + (1 - g_{VOR}) \cdot \dot{e}_{head} \quad (54)$$

In other words, depending on the gain of the VOR, the output of the PPRF can represent anything between an eye-in-head velocity signal ($G_{VOR} = 0$) and a gaze-velocity signal ($G_{VOR} = 1$)!

6.4 The Eye-Head Computer Model

For the brave and daring, there will be a Simulink implementation of the Goossens and Van Opstal (Figs. 49 and 50) model (in 1D and in 2D) available to the students.

Students may change several model parameters (within preset limits) and compare the models' behaviors to a range of different conditions (e.g. aligned vs. unaligned initial eye-head positions; VOR slow-phase gain; burst-generator dynamics; onset-disparities of eyes and head, etc.). Specific exercises will be handed out during the course.

After the simulation session, the tutors initiate a panel discussion with the audience that focuses on differences and similarities of the presented modeling approaches. Students are particularly encouraged to forward their own suggestions for specific topics.

6.5 Gaze-control model 1: Goossens-Van Opstal (GVO97)

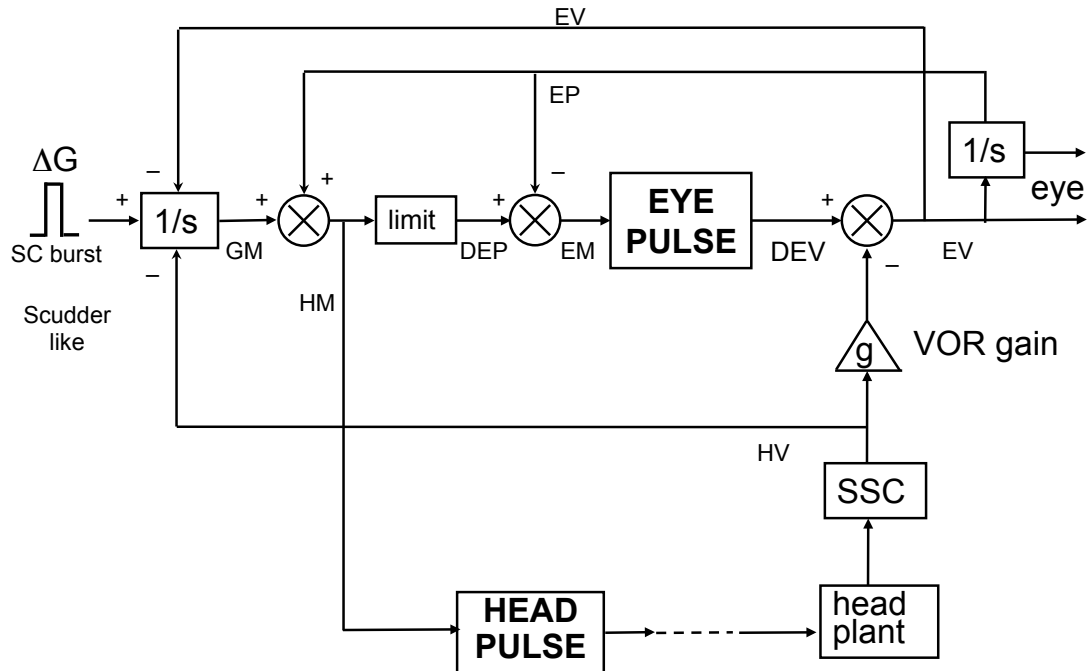


Fig. 49 Gaze-control model (1D) based on the head-fixed Scudder model of Fig. 27 (adapted from Goossens and Van Opstal, EBR, 1997). The SC provides a burst to the brainstem encoding desired gaze amplitude. The LLBNs integrate the difference between the SC output (desired gaze velocity) and efference copies of eye- and head velocities, yielding dynamic gaze-motorerror. The PPRF is driven by a desired (dynamic) eye-in-head position signal, which is the difference between gaze motorerror and current eye position. The Head BG is driven by (dynamic) head motor error. Note that the output of the Vestibular Nucleus (the slow-phase VOR) is subtracted from the PPRF output.

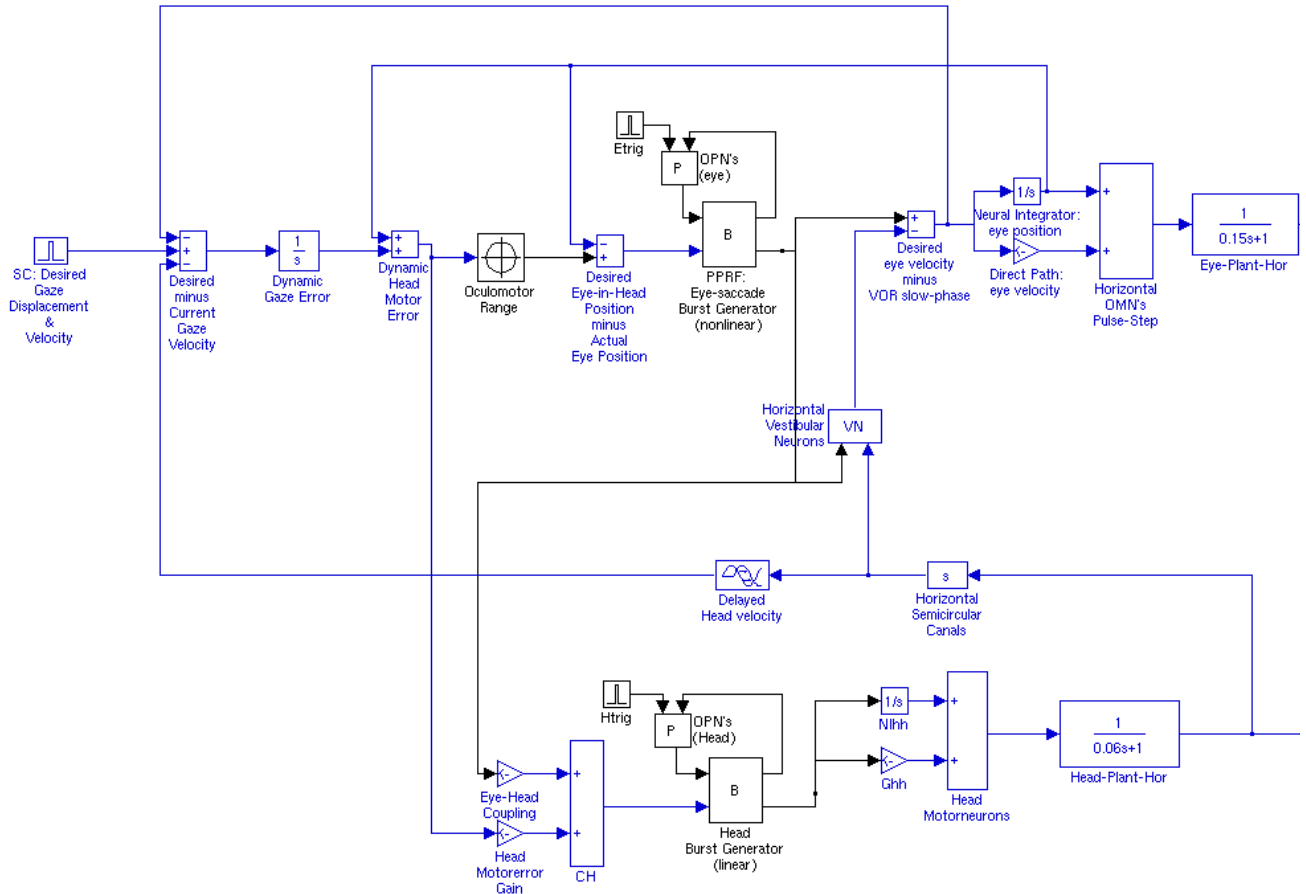


Fig. 50 Simulink implementation (*GVO97_1DMod.mdl*) of the GVO97 model in Fig. 49 that will be used in this afternoon's practicum. A 2D version of the GVO97 model will also be available for the real sturdy among the students (*GVO97_2DMod.mdl*).

6.6 Appendix: Parameter listings of Simulink Gaze Models

GVO97_1DMod.mdl		
Par	units	Description/values
Target/Eye		
TarHor	deg	horizontal gaze-target location. Default: 50
TarOn	sec	Target onset time; Def.: 0.1
SacOn	sec	Onset saccade (OPN offset). Def: 0.115
PBe	deg	Bias Omnipause Neurons Eye. Def: 5
dL	msec	Onset timing difference Eye-Head. Def: 40
OMRh	deg	Oculomotor Range (abs. value). Def: 40
Vmax	deg/s	Saturation level Eye BG nonlinearity; Def: 500
VT _e	ms	Time constant. Def: 0.001
Ao	deg	Angular constant Eye BG nonlinearity; Def.: 15
Te	sec	Time constant 1st-order eye plant. Def: 0.15
EHo	deg	Initial eye position. Def: 0
Head		
GH _h	gain	Input gains. Def: 1.0
Ch	gain	Eye (BG)-head (HME) coupling gain. Def.: 0.1
VG _h	deg	Angular constant Head BG. Def: 5
VSh	deg/s	Saturation level Head BG. Def: 10000
B VTh	sec	Time constant. Def: 0.001
PB _h	deg	Bias Head pausers. Def: 100
T1h,T2h	sec	Time constants 2nd-order head plant. Def: [0, 0.06]
Kh	gain	head plant damping coefficient. Def: 1.0
HHo	deg	Initial head position. Def: 0
VOR		
VORmax	gain	maximal gain VOR. Def: 1.0
VORmin	gain	minimal gain VOR. Def.: 0.5
VFD	sec	Delay vestibular feedback. Def: 0.005

1D "Scudder" version of the GVO97 model

GVO97_2DMod.mdl		
Par	units	Description/values
Target/Eye		
TarHor, TarVer	deg	horizontal/vertical gaze-target. Defaults: [30, 0]
TarOn	sec	Target onset time; Def.: 0
SacOn	sec	Onset saccade (OPN offset). Def: 0.1
PBe	deg	Bias Omnipause Neurons Eye. Def: 45
dL	msec	Onset timing difference Eye-Head
OMRh, OMRv	deg	Oculomotor Range (abs. value). Def: [40, 40]
Vmax	deg/s	Saturation level Eye BG nonlinearity; Def: 500
Ao	deg	Angular constant Eye BG nonlinearity; Def.: 15
Te	sec	Time constant 1st-order eye plant. Def: 0.15
EHo, EVo	deg	Initial eye position. Def: [0,0]
Head		
GHh, GHv	gain	Input gains. Def: [1.0, 0.7]
Ch, Cv	gain	Eye (BG)-head (HME) coupling gains. Def.: [0.1, 0.1]
VGh	deg	Angular constant Head BG. Def: 5
VSh	deg/s	Saturation level Head BG. Def: 10000
B VTh	sec	Time constant. Def: 0.001
PBh	deg	Bias Head pausers. Def: 80
T1h, T2h	sec	Time constants 2nd-order head plant. Def: [0, 0.06]
Kh	gain	head plant damping coefficient. Def: 1.0
HHo, HVo	deg	Initial head position. Def: [0, 0]
VOR		
VORmax	gain	maximal gain VOR. Def: 1.0
VORmin	gain	minimal gain VOR. Def.: 0.5

The full 2D version of the GVO97 gaze control model, as described in the EBR paper.

6.7 Looking inside OMR, BG and VOR

Figures 51 - 53 show how the Oculomotor Range (Fig. 51), the nonlinear Burst Generators (Fig. 52) and the dynamic VOR (Fig. 53) have been implemented in the two-dimensional version of the GVO97-model. The EOMR box receives two inputs: horizontal and vertical desired eye position in the head. The C2P ('Cartesian-to-Polar') block then converts the $[dEh, dEv]$ coordinates to the desired Eye Amplitude and Direction ($[R, \theta]$). The eye amplitude is then fed through the saturation function (circular-symmetric), yielding the actual desired eye-amplitude signal, after which the resulting polar coordinates are transformed back by the P2C block ('Polar-to-Cartesian'). The desired horizontal and vertical eye-in-head positions are the drive to the oculomotor burst generators.

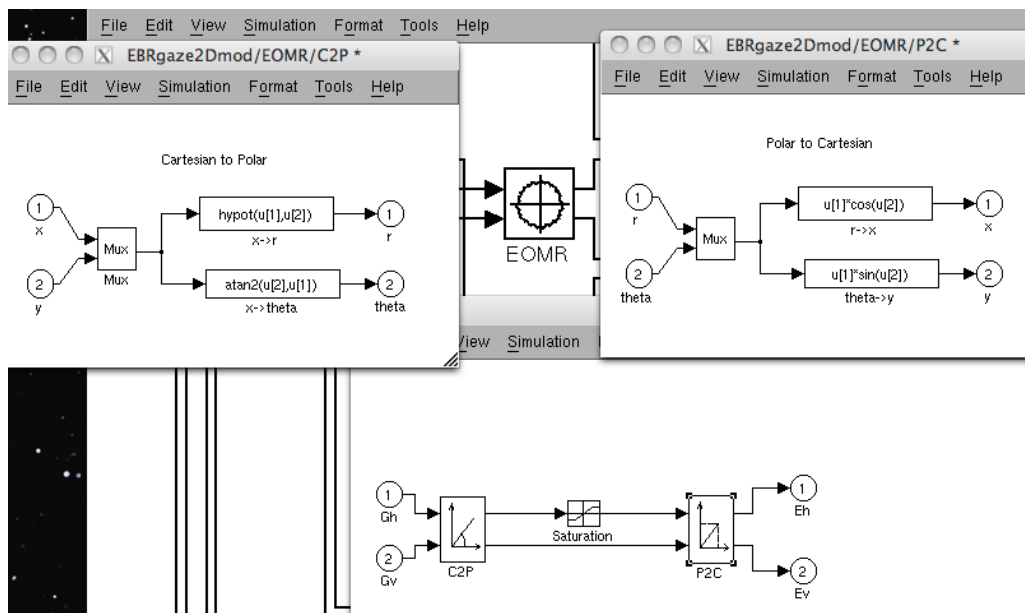


Fig. 51: Simulink implementation of the 2D oculomotor range.

The BNe block embeds the oculomotor burst generator, which is also implemented as a 2D vectorial operation. Inputs to the BG are the horizontal and vertical dynamic eye motor errors (Mh, Mv) (computed as the difference between the desired eye position from the OMR block output minus the current eye position), and the inhibitory bias from the OmniPause Neurons ("Inhibition"). The Cartesian motor error is transformed into a polar vector representation: $([R, \theta])$. The saturation is just a safety measure here (R between 0 and V_{max}). The amplitude of the dynamic motor error is then fed through the nonlinear saturating function (fcn) of Eqn. 49. The low-pass filter with the 1 ms time constant is inserted for numerical stability reasons only. The block yields three outputs: an inhibitory signal to the OPNs, to keep the gate closed during the saccade, and (after P2C) horizontal and vertical (desired) eye velocities. The latter are also fed to the head-motorerror input stage, as a (small) cross-coupling influence on the head.

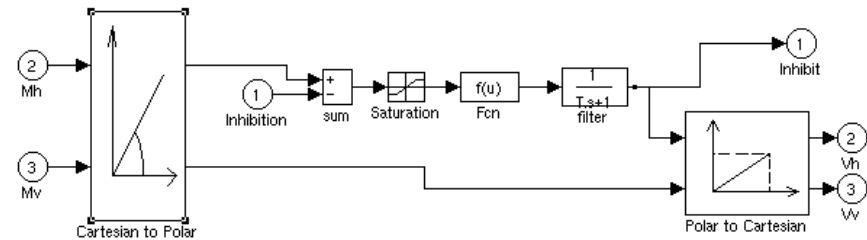
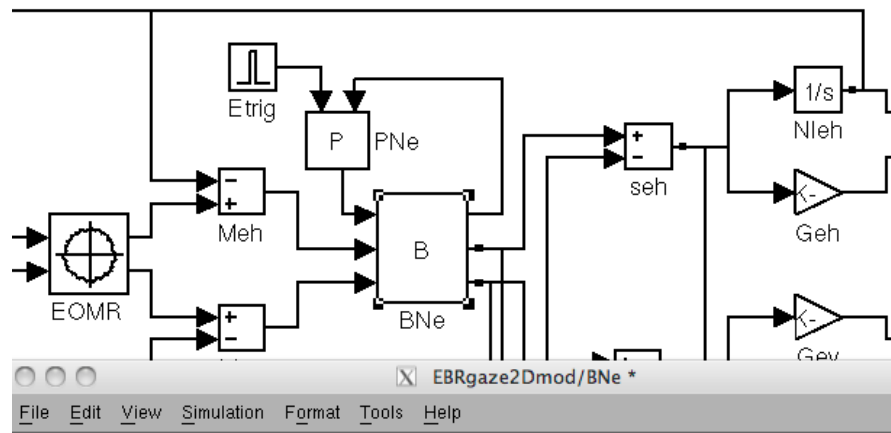


Fig. 52: Simulink implementation of the 2D burst generator.

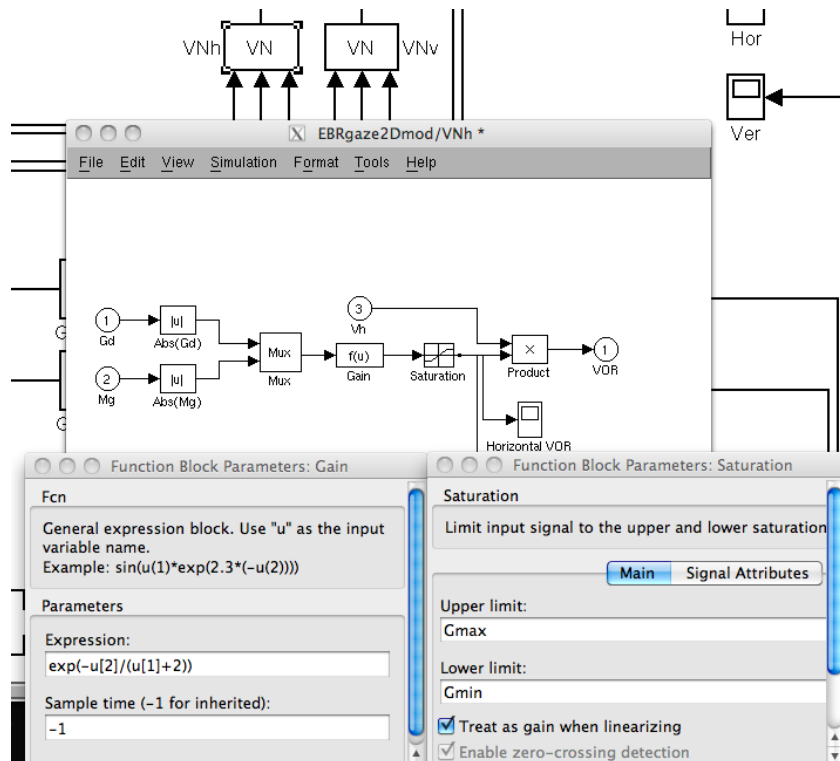


Fig. 53: Simulink implementation of the VOR.

The VN blocks implement the operation of the VOR before, during and after the gaze shift. The VN-block receives three inputs: the desired gaze displacement (nr. 1), the dynamic gaze motor error (nr. 2), and head velocity from the semicircular canals (nr. 3). The computation sets the gain of the VOR by normalizing the dynamic gaze-error. The $f(u)$ block takes the ΔG and $gme(t)$ inputs and computes:

$$g_{VOR}(t) = \exp\left(-\frac{gme(t)}{\Delta G + 2}\right)$$

which reduces the VOR gain to values between $1/e \approx 0.37$ for large gaze motor errors, to 1.0 when the gaze error approaches zero. The subsequent saturation function actually limits the change in VOR gain to values between 0.5 (VORmin) and 1.0 (VORmax). This gain is subsequently multiplied with the current head velocity, to yield the VOR output signal. See Fig. 51 for the details.

6.8 Scudder's model revisited: GVO2011

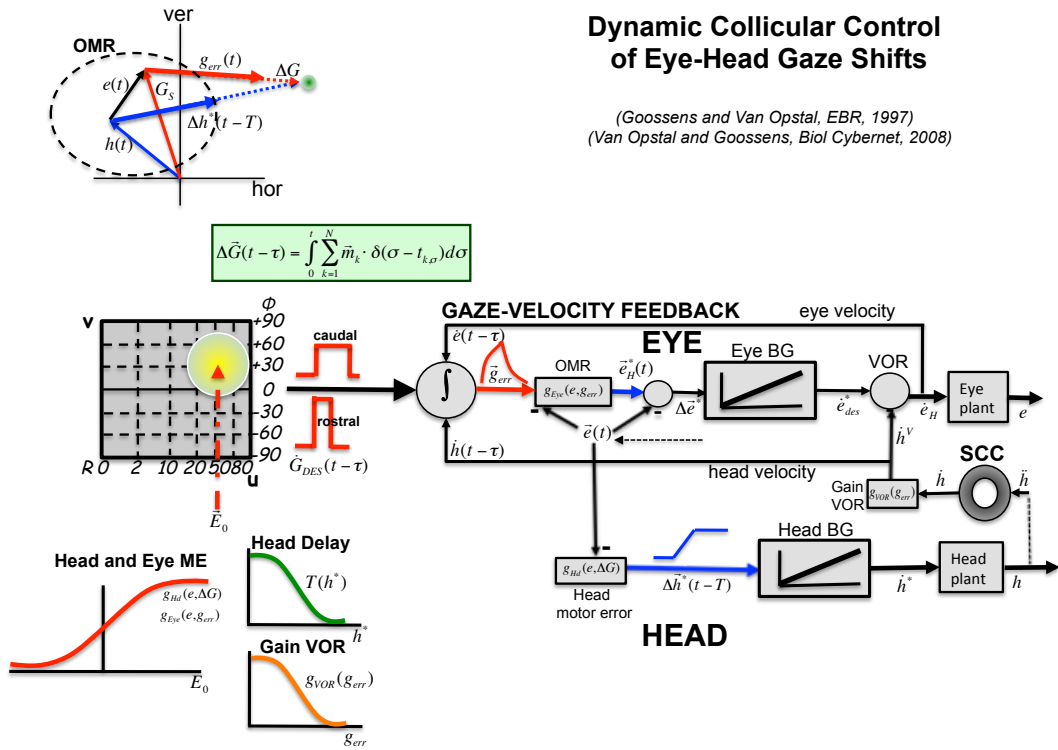


Fig. 54 Collicular eye-head gaze control, according to the spike-count hypothesis of G-VO (JNP, 2006). The Scudder version of Figs. 49-50 is modernized as follows: (i) the SC output specifies desired gaze velocity by firing rate, and current gaze displacement, $\Delta G(t)$, by the cumulative number of spikes in the population. (ii) the SC acts as a vectorial gaze burst generator that includes the main sequence. (iii) The eye- and head burst generators are taken to be linear. (iv) The main sequence relations are encoded by the SC through a rostral-caudal gradient in the burst properties: rostral cells (small gaze shifts) have higher firing rates and shorter burst durations than caudal cells (large gaze shifts). The equation (green box) explains how each spike, σ , in the burst of cell k at time $\tau_{\sigma,k}$, i.e., $\delta(t - \tau_{\sigma,k})$, contributes a fixed minivector, \vec{m}_k , to the brainstem that only depends on its location (u, v) in the motor map.

7 Selected references

1. Bergeron A, Guitton D, Fixation neurons in the superior colliculus encode distance between current and desired gaze positions. *Nat Neurosci* 3:932-939, 2000.
2. Bergeron A, Guitton D, In multiple-step gaze shifts: omnipause (OPNs) and collicular fixation neurons encode gaze position error; OPNs gate saccades. *J Neurophysiol* 88:1726-1742, 2002.
3. Choi WY, Guitton D, Responses of collicular fixation neurons to gaze shift perturbations in head-unrestrained monkey reveal gaze feedback control. *Neuron* 50:491-505, 2006.
4. Freedman E.G., Interactions between eye and head control signals can account for movement kinematics. *Biol. Cybernetics* 84, 453-462, 2001
5. Galiana H.L., A nystagmus strategy to linearize the vestibulo-ocular reflex, *IEEE Trans. Biomed. Eng.* 38 (6): 532-543, 1991.
6. Goossens H.H.L.M. and Van Opstal A.J., Human eye-head coordination in two dimensions under different sensorimotor conditions. *Exp Brain Res*, 114: 542-560, 1997
7. Goossens H.H.L.M. and Van Opstal A.J., Blink-perturbed saccades in monkey. II. Superior Colliculus activity. *J Neurophysiol*, 83, 3430-3452, 2000
8. Goossens H.H.L.M. and Van Opstal A.J., Dynamic Ensemble Coding of Saccades in the Monkey Superior Colliculus. *J Neurophysiol*, 95: 2326-2341, 2006
9. Guitton D., Munoz D.P. and Galiana H.L., Gaze control in the cat: Studies and modelling of the coupling between orienting eye and head movements in different behavioral tasks, *J. Neurophysiol* 64: 509-531 1990.
10. Kardamakis AA, Moschovakis AK, Optimal control of gaze shifts. *J Neurosci* 29:7723-7730, 2009.
11. Khojasteh E. and H.L. Galiana, Primate disconjugate eye movements during the horizontal AVOR in darkness and a plausible mechanism, *Exp Brain Res* 198: 1-18, 2009.
12. Khojasteh E. and H.L. Galiana, Implications of gain modulation in brainstem circuits: VOR control system, *J. Computational Neuroscience* 27: 437-451, 2009.
13. Lefevre P., Galiana H.L. Dynamic feedback to the superior colliculus in a neural network model of the gaze control system. *Neural Networks* 5: 871-890, 1992.
14. Mettens P. , Godaux E., Cheron G., Galiana H.L. , Effect of muscimol microinjections into the prepositus hypoglossi and the medial vestibular nuclei on cat eye movements, *J. Neurophysiol.* 72 (2): 785-802, 1994.
15. Paré M, Guitton D, Brainstem omnipause neurons and the control of combined eye-head gaze saccades in the alert cat. *J Neurophysiol* 79:3060-3076, 1998.
16. Prsa M. and H.L. Galiana, A visual-vestibular interaction hypothesis for the control of orienting gaze shifts by brainstem omnipause neurons, *J. Neurophysiol.* (Feb) 97: 1149-1162, 2007
17. Roy JE, Cullen KE (2004) Dissociating self-generated from passively applied head motion: neural mechanisms in the vestibular nuclei. *J Neurosci* 24:2102-2111.
18. Scudder C.A., A new local feedback model of the saccadic burst generator. *J. Neurophysiol.* 59: 1455-1475, 1988

19. Scudder CA, Fuchs AF, Physiological and behavioral identification of vestibular nucleus neurons mediating the horizontal vestibuloocular reflex in trained rhesus monkeys. *J Neurophysiol* 68:244-264, 1992.
20. Scudder CA, Kaneko CRS, Fuchs AF, The brainstem burst generator for saccadic eye movements: a modern synthesis. *Exp Brain Res* 142:439-462, 2002.
21. Smith H.L. and Galiana H.L., The role of central bilateral symmetry in linearizing the vestibuloocular reflex, *Biol. Cybernetics*: 65, 11-22, 1991.
22. Sparks D.L. and Mays L.E., Spatial Localization of Saccade Targets. I. Compensation for Stimulation-Induced Perturbations in Eye Position. *J. Neurophysiol.* 49: 45-63, 1983
23. Sylvestre P.A., H.L. Galiana, K.E. Cullen, Conjugate and vergence oscillations during saccades and gaze shifts: Implications for the integrated control of binocular movements, *J. Neurophysiol.* 87: 257-272, 2002.
24. Sylvestre PA, Cullen KE, Premotor correlates of integrated feedback control for eye-head gaze shifts. *J Neurosci* 26:4922-4929, 2006.
25. Tomlinson RD, Bahra PS. Combined eye-head gaze shifts in the primate, II. Interactions between saccades and the vestibulocular reflex. *J Neurophysiol* 56:1558-1570, 1986.
26. Van Gisbergen JA, Robinson DA, Gielen S, A quantitative analysis of generation of saccadic eye movements by burst neurons. *J Neurophysiol* 45:417-442, 1981.
27. Van Opstal A.J. and Goossens H.H.L.M., Linear Ensemble Coding in Midbrain Superior Colliculus Specifies the Saccade Kinematics. *Biological Cybernetics*, 98: 561-577, 2008
28. Vliegen, J., Van Grootel T.J. and Van Opstal A.J., Dynamic sound localization during rapid eye-head gaze shifts. *J Neuroscience*, 24: 9291-9302, 2004
29. Vliegen, J., Van Grootel T.J. and Van Opstal A.J., Gaze Orienting in Dynamic Visual Double Steps. *J Neurophysiol*, 94: 4300-4313, 2005